Neuroscience 167 (2010) 1070–1090

THE DETERMINANTS OF THE ONSET DYNAMICS OF ACTION POTENTIALS IN A COMPUTATIONAL MODEL

G. BARANAUSKAS,[a] A. MUKOVSKIY,[b1] F. WOLF[c] AND M. VOLGUSHEV[b,d]*

[a]*Department of Robotics, Brain and Cognitive Sciences, The Italian Institute of Technology, Genova, Italy*

[b]*Department of Neurophysiology, Ruhr-University, Bochum, Germany*

[c]*Max-Planck-Institute for Dynamics and Self-Organization, Faculty of Physics, Georg-August-University and Bernstein Center for Computational Neuroscience, Göttingen, Germany*

[d]*Department of Psychology, University of Connecticut, Storrs, CT, USA*

Abstract—Action potentials (APs) in the soma of central neurons exhibit a sharp, step-like onset dynamics, which facilitates the encoding of weak but rapidly changing input signals into trains of action potentials. One possibility to explain the rapid AP onset dynamics is to assume cooperative activation of sodium channels. However, there is no direct evidence for cooperativity of voltage gated sodium channels in central mammalian neurons. The fact that APs in cortical neurons are initiated in the axon and backpropagate into the soma, prompted an alternative explanation of the sharp onset of somatic APs. In the invasion scenario, the AP onset is smooth at the initiation site in the axon initial segment, but the current invading the soma before somatic sodium channels are activated produces a sharp onset of somatic APs. Here we used multicompartment neuron models to identify ranges of active and passive cell properties that are necessary to reproduce the sharp AP onset in the invasion scenario. Results of our simulations show that AP initiation in the axon is a necessary but not a sufficient condition for the sharp onset of somatic AP: for a broad range of parameters, models could reproduce distal AP initiation and backpropagation but failed to quantitatively reproduce the onset dynamics of somatic APs observed in cortical neurons. To reproduce sharp onset of somatic APs, the invasion scenario required specific combinations of active and passive cell properties. The required properties of the axon initial segment differ significantly from the currently accepted and experimentally estimated values. We conclude that factors additional to the invasion contribute to the sharp AP onset and further experiments are needed to explain the AP onset dynamics in cortical neurons.

Key words: action potential, axon, simulations, Hodgkin–Huxley model, sodium channels, onset dynamics.

Action potentials (APs) recorded in the soma of central neurons exhibit a variable threshold and a very rapid, step-like onset dynamics (Naundorf et al., 2006; Yu et al., 2008). It has been shown that the sharp onset dynamics of APs facilitates the encoding of weak but rapid changes of neuronal inputs into the patterns of spikes (Fourcaud-Trocme et al., 2003; Naundorf et al., 2005). High temporal precision of AP generation is crucial for sensory information processing (e.g. reviews Buracas and Albright, 1999; Singer, 1999) as well as for the induction of synaptic plasticity (Markram et al., 1997; Magee and Johnston, 1997; Kampa et al., 2007). Thus, it is important to understand the mechanisms that determine the onset dynamics of central APs. The basic mechanisms of AP generation were described over 50 years ago in the seminal studies of Hodgkin, Huxley and Katz on the squid giant axon (Hodgkin and Huxley, 1952a,b; Hodgkin et al., 1952). The Hodgkin–Huxley model (HH model) has been used to reproduce a large number of neuronal biophysical phenomena, however it became clear during the subsequent years that kinetics of sodium and potassium channels in central neurons deviates from the canonical HH equations (e.g. Patlak, 1991; Hille, 2001; Baranauskas and Martina, 2006; Baranauskas, 2007). For APs initiated in the soma, the canonical HH model with independent sodium channels cannot account for the combination of a variable threshold and a rapid AP onset (Naundorf et al., 2006). Introduction of cooperative activation of sodium channels is sufficient to account for both the rapid onset dynamics and the high threshold variability of the neocortical APs (Naundorf et al., 2006). In the cooperative model, the probability of a sodium channel to open increases when a neighbor sodium channel is open. This model attributes the observed steep AP onset to this intrinsic channel property and thus predicts the same or very similar rapid onset of APs at the initiation site and in the soma. However, several recent studies have shown that the onset of APs recorded from the injury-induced swellings or "blebs" of the axons cut on the slice surface is smooth (Yu et al., 2008; McCormick et al., 2007; Shu et al., 2007; Schmidt-Hieber et al., 2008a; Hu et al., 2009). Although a cooperative activation has been demonstrated for several channels (Marx et al., 1998, 2001; Molina et al., 2006; Dekker and Yellen, 2006) including sodium channels from cardiac myocytes (Undrovinas et al., 1992), it is important to note that there is no direct evidence for cooperation between sodium channels in central neurons.

[1] Present address: Department of Cognitive Neurology, Hertie Institute for Clinical Brain Research, Centre for Integrative Neuroscience, University of Tübingen, Tübingen, Germany.

*Correspondence to: M. Volgushev, Department of Psychology, University of Connecticut, 406 Babbidge Road Unit 1020, Storrs, CT 06269-1020, USA. Tel: +1-860-486-6825; fax: +1-860-486-2760.
E-mail address: maxim.volgushev@uconn.edu (M. Volgushev).

Abbreviations: AIS, axon initial segment; AP, action potential; BM model, Baranauskas, Martina model of sodium channels; C_m, membrane capacitance; G_{Leak}, leak conductance; gNa, maximal sodium conductance; HH model, Hodgkin–Huxley model; I_{Ca}, high voltage activated Ca^{2+} current; I_{KCa}, calcium dependent potassium current; I_{Km}, slow non-inactivating potassium current; I_{kv}, rapid potassium conductance; Rax, cytoplasmic resistance.

0306-4522/10 $ - see front matter © 2010 IBRO. Published by Elsevier Ltd. All rights reserved.
doi:10.1016/j.neuroscience.2010.02.072

Subsequently, it was suggested that the rapid AP onset in the soma of neocortical neurons is a consequence of AP initiation in the axon that then backpropagates into the soma (McCormick et al., 2007; Yu et al., 2008). In cortical neurons APs are initiated not in the soma but in the axon initial segment (AIS) or the first node of Ranvier (Stuart and Häusser, 1994; Stuart and Sakmann, 1994; Colbert and Johnston, 1996; Clark et al., 2005; Meeks et al., 2005; Khaliq and Raman, 2006; Palmer and Stuart, 2006; Kress et al., 2008; Schmidt-Hieber et al., 2008a). In layer 5 neocortical pyramidal neurons, APs are initiated ~25–40 μm away from the soma (Palmer and Stuart, 2006). In the invasion scenario (McCormick et al., 2007; Yu et al., 2008) an AP generated at the initiation site has a slow onset, in accordance with the canonical Hodgkin–Huxley type kinetics. However, in the soma, the invasion of the axonal AP leads to a rapid depolarization of the membrane from the baseline voltage and thus the appearance of a "kink" at the onset of the somatic AP. Indeed, APs initiated in the "blebs" of the cut axons have a smooth Hodgkin–Huxley type onset, clearly different from the onset of somatic APs (McCormick et al., 2007; Shu et al., 2007; Yu et al., 2008; Schmidt-Hieber et al., 2008a; Hu et al., 2009). It has been suggested that, since "the kink and increased spike threshold variability arises from the recording of action potentials distal to their site of generation, every model that initiates spikes at a distance exhibited these basic properties" (Yu et al., 2008, p. 7271). However, this conclusion may actually hold only for the models tested in Yu et al. (2008) and with the criteria they used. Indeed, some previously described models of distal AP initiation show smooth onset of somatic APs (e.g. Colbert and Pan, 2002; Schmidt-Hieber et al., 2008a). Further, some direct recordings from the axon do not find such clear-cut differences between the onset of AP at the initiation site and in the soma (Stuart et al., 1997a,b). Moreover, we find that the onset rapidness criteria chosen by Yu et al. (2008), can discriminate well between a step-like and a smooth AP onset only if measured close to the threshold, but when measured further away from the AP threshold, the rapidness becomes similar for APs with the rapid and the slow onsets (see the results section in this paper).

Thus, to resolve this controversy and identify the ranges of model parameters that can reproduce the sharp onset of somatic APs in the invasion scenario, we performed computer simulations and explored the influence of active and passive cell properties on AP onset dynamics. We employed a recently described measure of AP onset dynamics that allows a more rigid quantitative comparison of AP onset dynamics in simulations and in traces obtained from real neurons (Volgushev et al., 2008). For simulations we used two Hodgkin and Huxley-type sodium channel models, the canonical HH-model (Hodgkin and Huxley, 1952a,b; Hodgkin et al., 1952; Dayan and Abbott, 2001; Hille, 2001) and the one modified according to Baranauskas and Martina (2006, BM-model). Our results show that, for a broad range of channel densities and other cellular parameters, somatic APs have a smooth onset despite their backpropagation from the AIS to the soma. Thus, backpropagation of an AP from the AIS into the soma represents a necessary but not sufficient condition to explain the rapid onset of somatic AP in the invasion scenario.

EXPERIMENTAL PROCEDURES

Simulations were performed in NEURON environment (http://www.neuron.yale.edu/neuron/ version 5.8, Hines et al., 2004; Carnevale and Hines, 2006). Integration time step was 0.01 ms (100 kHz) in all simulations. Before starting main simulation series, we made several preliminary runs with smaller or longer integration time step (0.02–0.005). Results obtained with integration time steps in that range did not differ significantly, which is not surprising because NEURON implements a rather stable integration algorithm (Hines et al., 2004).

Model morphology

Our basic model, used for the majority of simulations had a reduced dendritic structure, but realistic morphology of the initial portion of the axon (Fig. 1A). An "apical" dendrite (200 μm long, tapering from 4 to 1 μm, 16 segments) with two 90 μm long branches and two "basal" dendrites (70 μm long, tapering from 2 to 0.5 μm, five segments) were attached to a 25 μm wide and 35 μm long soma (five segments). The axon consisted of a 10 μm hillock (two segments), tapering from 4 to 1.2 μm, proximal and distal initial segments (AIS), each 20 μm long (four segments) and 1.2 μm thick, followed by 10 myelinated sections (each 98 μm long, 1.2 μm thick, eight segments) with nodes of Ranvier (2 μm long, 1.1 μm thick), and a non-myelinated terminal (100 μm long, tapering from 1.2 to 0.1 μm, eight segments). To test if segmentation of the initial part of the axon is sufficient, we run several tests with increased number of segments (up to 20) in the axon hillock and AIS. This did not change simulation results significantly, so we believe that our segmentation scheme did not influence the conclusions reached in this study. Axon geometry in our model conforms to the published results of morphological reconstructions and reproduces typical dimensions of the initial portion of the axon reported for layer 5 pyramidal cells in the neocortex, for example (Sloper and Powell, 1979; Miller and Peters, 1981; Mainen et al., 1995; Mainen and Sejnowski, 1996; Palmer and Stuart, 2006). The same or similar values were used in published morphologically realistic models based on morphological reconstructions, for example (Mainen et al., 1995; Mainen and Sejnowski, 1996; Kole et al., 2008). To study the influence of the axon morphology on the AP dynamics, we have modified the diameter of the AIS between 0.8 and 1.8 μm, and its length from 40 to 70 μm. These values cover the low end of the reported AIS diameters and the limits of reported AIS length (Peters et al., 1968; Sloper and Powell, 1979; Miller and Peters, 1981; Bragina, 1986).

Passive properties of the cell cytoplasm and membrane were initially set according to the commonly used values and later changed to cover all range of values suggested by different studies. Axial resistance Rax of the cell cytoplasm was initially set to 150 Ohm×cm and later tested at 50–450 Ohm×cm (Roth and Wikswo, 1985; Stuart and Spruston, 1995; Bekkers and Stevens, 1996; Meyer et al., 1997; Stuart and Spruston, 1998; Trevelyan and Jack, 2002). Leak conductance G_{Leak} of the cell membrane was set at 0.2 pS/μm^2, corresponding to the input resistance of the simulated cell Rm at rest of about 400 MOhm. Myelinated sections of the axon, because of shielding effect, had lower membrane conductance of 0.004 pS/μm^2. We also used an about 16 times higher value for the leak conductance, 3.3 pS/μm^2, corresponding to the cell input resistance of 35 MOhm that would mimic much higher somatic/dendritic conductance load as suggested in (Yu et al., 2008). Reversal potential for the leak conductance was

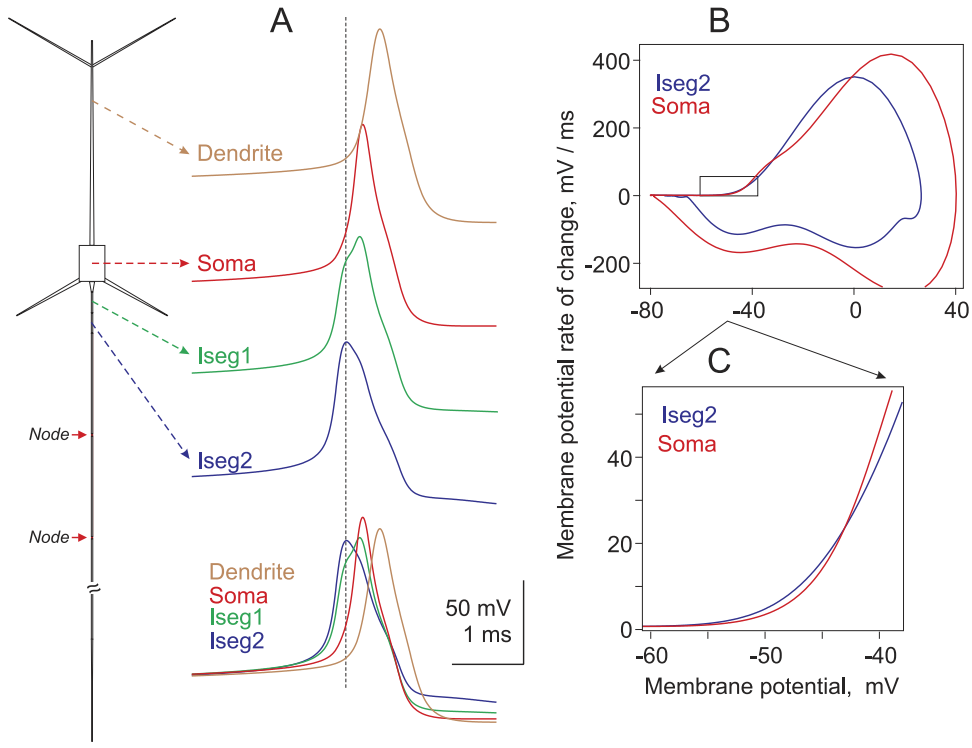

Fig. 1. Action potential (AP) initiation in a neuron model with a simple geometry. (A) Model neuron geometry and the AP in different compartments, generated by the model neuron in response to somatic current injection. Models of the same geometry were used for all simulations in this study, except when stated otherwise. The AP is initiated in the initial segment 2 (Iseg2) and propagates in both directions: down the axon, and towards the soma and dendrites. Vertical interrupted line shows the peak of the AP in the initial segment 2. In the lower panel, APs recorded from different compartments are superimposed. In this and all other models of this geometry, sodium channels in the AIS had negatively shifted activation curve. In this model, density of sodium channels in the AIS was three times higher than in the soma, as demonstrated with direct measurements in membrane patches from the soma and axon initial segment (Colbert and Pan, 2002; Kole et al., 2008). (B) Phase plot of the APs at the initiation site (Iseg2, blue) and in the soma (red). (C) Initial portion of the APs from (B) at higher magnification. Note that despite initiation in the distal initial segment and backpropagation, the AP in the soma has a smooth onset. For interpretation of the references to color in this figure legend, the reader is referred to the Web version of this article.

−80 mV. Membrane capacitance C_m was set at 1.0 μF/cm^2 everywhere except for the myelinated axon sections in which it was 0.02 μF/cm^2. Virtual temperature was 32 °C for most of the simulations, but several models were tested at temperatures from 10 to 37 °C. To account for temperature dependence of passive neuron properties shown *in vivo* and *in vitro* (Klee et al., 1974; Thompson et al., 1985; Volgushev et al., 2000a,b; Trevelyan and Jack, 2002), we implemented quantitative dependencies obtained by fitting parameters of neuron models to experimental data (Trevelyan and Jack, 2002). For the membrane capacitance C_m Q_{10} was 0.96; for the axial resistance Rax Q_{10} was 0.8 and for the leak conductance G_{Leak} Q_{10} was 1.97. Note that the ranges of passive properties studied here (9-fold for Rax and 16-fold for G_{Leak}) were broader than possible ranges due to temperature changes.

Voltage-gated sodium conductance

Standard equations were used for the Hodgkin–Huxley model of sodium channels (Hodgkin and Huxley, 1952a,b; Hodgkin et al., 1952; Dayan and Abbott, 2001). The script (Mainen et al., 1995; Mainen and Sejnowski, 1996) was downloaded from SenseLab's ModelDB database URL: http://senselab.med.yale.edu/senselab/modeldb. The activation and inactivation midpoint for sodium channels was −35 and −65 mV respectively in all cell compartments except for the initial segments where the activation midpoint was −43 mV while the inactivation $V_{1/2}$ was unchanged (see below). Equilibrium potential for Na^+ ions, E_{Na}, was set to 60 mV.

Since recent experimental results showed that kinetics of sodium channels in central neurons cannot be captured by canonical HH scheme, we have also used a modified kinetics (Baranauskas and Martina, 2006) (BM sodium channels), available at http://senselab.med.yale.edu/senselab/modeldb. In brief, this model has six states: one open state, two closed states and three inactivated states. The transition rates from the second closed state to the open state (α2 and β2) and all transition rates to the inactivated states (α3 and β3, the same for all transitions to an inactivated state) were obtained directly from sodium current fits. It was assumed that all these rates saturate except for β3. The following functions describe the voltage dependence of these rate constants:

$$\alpha 2 = 2.8^{((T-13)/10)} \times 11/(4+\exp(-(V+6)/12))$$

$$\beta 2 = 2.8^{((T-13)/10)} \times 0.035/(0.0015+\exp((V+6)/12))$$

$$\alpha 3 = 2.4^{((T-13)/10)} \times 2/(2+\exp(-(V+6)/12))$$

$$\beta 3 = 2.4^{((T-13)/10)} \times 0.00005 \times \exp(-(V+6)/13)$$

Here T stands for temperature in °C, V stands for membrane voltage in mV, the rate constants' units are ms^{-1}.

The transition from the first to the second closed state helps to account for the observed steep voltage dependence of the sodium current amplitude and the presence of a very brief delay in the current onset (<0.2 ms at 12 °C). Therefore, α1 was adjusted to reproduce the current amplitudes observed during voltage clamp

recordings at <−40 mV while maintaining the slowest time constant of this transition <0.2 ms. The following rates were used in the model:

$$\alpha 1 = 2.8^{((T-13)/10)} \times 10 \times \exp((V+6)/45)$$

$$\beta 1 = 2.8^{((T-13)/10)} \times 0.35 \times \exp(-(V+6)/8)$$

In the BM model, sodium channel conductance density is expressed in permeability terms, the standard permeability of soma used here was 0.5×10^{-4} cm/s that corresponds to approximately 100 pS/μm^2 (Baranauskas and Martina, 2006).

Recently, modifications of the Hodgkin and Huxley model of sodium channels with faster activation and inactivation kinetics were suggested for layer 5 pyramidal cells (Kole et al., 2008) and unmyelinated axons (Engel and Jonas, 2005). We tested these models and found that although activation kinetics of the Engel and Jonas (2005) model is much faster than in canonical HH model, it is not faster than in the BM model (Supplementary Fig. S1). Moreover, the AP onset is slower in simulations employing this model than the BM model. This may be attributable to much faster inactivation kinetics of sodium channels in Engel and Jonas (2005) model (Supplementary Fig. S1). These results show that the HH and BM models represent two extremes of the sodium channel models suggested to reproduce sodium current kinetics in central neurons and thus cover the whole range of models found in the current literature. Therefore, we limited our simulations to the HH and BM models of sodium channels.

Experimental data show that sodium channels in the distal AIS are activated at 7–15 mV more hyperpolarized potentials than somatic channels (Colbert and Pan, 2002; Schmidt-Hieber et al., 2008b; Kole and Stuart, 2008; Hu et al., 2009). In accordance with these data, we have used in our models a negative 8 mV shift of the activation curve of sodium channels in the AIS relative to the activation of sodium channels in other parts of the cell. With this shift, APs were initiated in the initial segment and backpropagated to the soma even in models with moderate channel density in the AIS, only three times higher than in the soma. According to (Colbert and Pan, 2002; Kole et al., 2008; Lorincz and Nusser, 2008) the density of sodium channels increases towards the distal AIS, but not immediately in the axon hillock. To account for these data, the density of sodium channels in the axon hillock was intermediate between the soma and the AIS, 50% of that in the AIS. We used neuron models in which the density of sodium channels in the AIS varied from 3 to 900 times higher than in the soma.

Potassium conductance

Two types of potassium conductance were used in simulations: fast and slow delayed rectifier. The fast potassium conductance corresponded to the classical HH delayed rectifier current taken from (Mainen et al., 1995; Mainen and Sejnowski, 1996) but the activation midpoint was shifted from ~ +6 mV to more hyperpolarized potential (−25 mV), which is closer to the original HH model (Hodgkin and Huxley, 1952a,b; Hodgkin et al., 1952) and the recent data of on potassium channels in the AIS (Kole et al., 2007). The model script (Mainen et al., 1995; Mainen and Sejnowski, 1996) was downloaded from SenseLab's ModelDB database and the file was re-written for clarity and some errors were corrected (*n***4, not *n***1 as in the MS script). In the basic model, the density of this current was set to 1000 pS/μm^2 (0.1 S/cm^2) in the axon initial segment, 400 pS/μm^2 (0.04 S/cm^2) in the soma and 200 pS/μm^2 (0.02 S/cm^2) in the dendrites. To test the hypothesis that high potassium channel density in the AIS may affect the onset dynamics of AP in the soma, the density of the fast potassium conductance was increased in some simulations 30 fold (to 30,000 pS/μm^2=3 S/cm^2) in the axon initial segment.

The slow potassium channels reproduce the slow delayed rectifier current found in cortical neurons (Korngreen and Sakmann, 2000; Baranauskas, 2007). This current was added to reproduce the relatively slow recovery of membrane potential after an AP in cortical neurons. The model of these channels has six states: one open state, two closed states and three inactivated states as in the BM model of sodium channels. Rate constants $\alpha1$ and $\beta1$ correspond to the transitions from the first closed or inactivated state to the second closed or inactivated state while rate constants $\alpha2$ and $\beta2$ correspond to the transitions from the second closed or inactivated state to the open or third inactivated state. Slow inactivation of potassium current was described by rate constants $\alpha3$ and $\beta3$ (all transitions from either any closed state or the open state to the corresponding inactivated state).

The following functions describe the voltage dependence of these rate constants:

$$\alpha 1 = 2.8^{((T-23)/10)} \times 3/(0.3+15\times\exp(-V/25))$$

$$\beta 1 = 2.8^{((T-23)/10)} \times 3/(1+12\times\exp(V/25))$$

$$\alpha 2 = 2.8^{((T-23)/10)}/(5+13\times\exp(-V/13))$$

$$\beta 2 = 2.8^{((T-23)/10)}/(10+700\times\exp(V/20))$$

$$\alpha 3 = 2.4^{((T-23)/10)}/(5+6000\times\exp(-V/30))$$

$$\beta 3 = 2.4^{((T-23)/10)}/(15+50000\times\exp(V/25))$$

Here T stands for temperature in °C, V stands for membrane voltage in mV, the rate constants' units are ms^{-1}.

The density of the slow delayed rectifier current was 600 pS/μm^2 (0.06 S/cm^2) in the soma, 1200 pS/μm^2 (0.12 S/cm^2) in the AIS and 300 pS/μm^2 (0.03 S/cm^2) for dendritic compartments. The potassium ion reversal potential was set to −85 mV.

Our preliminary tests revealed no significant effects of A-type current on the AP onset dynamics although the AP threshold was strongly affected as expected. Since there is great variability in amplitude and kinetics of A-type current from cell to cell (Korngreen and Sakmann, 2000; Baranauskas, 2007; Yuan and Chen, 2006), this current was not included on our main simulation set.

Thus, the basic model contained only four conductances: leak conductance, voltage-gated sodium and two voltage-gated potassium conductances. Since for sub-threshold membrane potentials, the kinetics of voltage-gated sodium currents is about an order of magnitude faster than kinetics of any other conductance described so far (Hille, 2001; Baranauskas, 2007), this choice of conductances represents a reasonable simplification to study the onset dynamics of APs. In addition to these four basic conductances, we have also studied APs simulated with models implementing persistent Na^+ current, as well as a set of other conductances, including slow non-inactivating potassium current I_{Km}, high voltage activated Ca^{2+} current I_{Ca} and calcium dependent potassium current I_{KCa}, as used in published models, for example (Mainen et al., 1995; Mainen and Sejnowski, 1996).

For the models with either HH and BM type of sodium channels, we have varied the following parameters and/or their combinations (see also Table 1):

(a) The ratio of the maximal sodium conductance (gNa) in the AIS relative to the soma, from 3 to 900;
(b) The maximal Na^+ conductance (gNa) in the soma, 100, 300 and 900 pS/μm^2; and up to 270,000 pS/μm^2 in the AIS;
(c) The maximal density of the rapid potassium conductance (I_{Kv}) in the AIS, 1000 and 30,000 pS/μm^2, (0.1 and 3.0 S/cm^2) the latter value about 30 times higher than the usually used;
(d) Presence of persistent sodium current, 5% of the amplitude of the fast sodium current in the axon hillock and initial segment;
(e) Leak conductance, 0.2 pS/μm^2, and ~16 times higher, 3.3 pS/μm^2, to mimic the dendritic/somatic shunt as suggested in Yu et al. (2008);
(f) Cytoplasmic resistance, Rax, from 50 to 450 Ohm×cm;
(g) The diameter of the axon initial segment, from 0.8 to 1.8 μm;
(h) The length of the axon initial segment, 40 and 70 μm;
(i) Virtual temperature, from 10 to 37 °C.

Table 1. Parameters of the models used in this study

	Models with reduced morphology			Models with realistic morphology (Mainen and Sejnowski, 1996)[a] Sodium and fast potassium channels as in:		
	Basic model	Parameter range tested	Yu et al. (2008), "Simple model"	Mainen, Sejnowski, 1995, 1996	Destexhe et al. 1999, 2001	Colbert, Pan 2002[b]
Sodium conductances						
gNa, soma, pS/μm^2	100	100 . . . 900	800	20	120	1000[b]
gNa, AIS, pS/μm^2	500	300 . . . 270,000	8000	30,000	1200	3000[b]
Ratio gNa, AIS/soma	5	3 . . . 900	10	1500	10	3[b]
Persistent Na current, % of gNa	0	0, 5	—	—	—	—
Fast potassium conductances						
I_{kv}, soma, pS/μm^2	400		320	200	100	200
I_{kv}, AIS, pS/μm^2	1000	1000 . . . 30,000	1500	2000	1000	2000
Passive properties						
Rax, Ohm$\times$cm	150	50 . . . 450	150	200	150	150
G_{Leak}, pS/μm^2	0.2	0.2, 3.3	0.33	0.33	0.33	0.33
Membrane capacitance						
C_m, μF/cm^2	1.0[c]		0.75	0.75	0.75	1.0
Axon geometry						
Axon hillock, μm	10		—	10	10	10
AIS diameter, μm	1.2	0.8 . . . 1.8	1.0	1.479[d]	1.479[d]	1.479[d]
AIS length, μm	40	40, 70	50	15	15	30
Axon beyond AIS, μm	1100		—	510	510	510
Temperature, °C	32	10 . . . 37	32	32	32	32

References for Table 1: (Yu et al., 2008; Mainen and Sejnowski, 1996; Destexhe and Pare, 1999; Destexhe et al., 2001; Colbert and Pan, 2002).
[a] L5 and L3 pyramids; L3 aspiny cell; L4 spiny stellate.
[b] Activation shift of AIS sodium channels and ratio of AIS/soma channels as in Colbert and Pan (2002).
[c] In myelinated axon sections Cm=0.02 μF/cm^2.
[d] L5 pyramid; 0.99 for L3 pyramid; 0.52 for L3 aspiny cell; 0.79 for L4 spiny stellate.

In theory, the complex geometry of neocortical neuron dendrites and axons could alter the dynamics of action potential propagation and backpropagation. To account for that possibility, we used several models with realistic geometry of neocortical neurons (Mainen et al., 1995; Mainen and Sejnowski, 1996): layer 3 pyramid; layer 3 aspiny cell; layer 4 stellate cell and layer 5 pyramidal neuron, downloaded from SenseLab's ModelDB database URL: http://senselab.med.yale.edu/senselab/modeldb, either with original settings or with channel distributions suggested in other studies (Destexhe and Pare, 1999; Destexhe et al., 2001; Colbert and Pan, 2002; Kole et al., 2008). These models also included a larger number of ionic currents, for example slow non-inactivating potassium current I_{Km}, high voltage activated Ca^{2+} current I_{Ca} and calcium dependent potassium current I_{KCa}, as specified in (Mainen et al., 1995; Mainen and Sejnowski, 1996) and in respective NEURON scripts.

Finally, we also tested a "simple" model, recently suggested by Yu and colleagues (Yu et al., 2008) to explain the fast onset of somatic APs in large layer 5 pyramids in the neocortex. This model consisted of three compartments: a 30$\times$20 μm^2 soma, a 1 μm thin 50 μm long axon initial segment attached directly to the soma from one side, and a 5 μm thick 3000 μm long dendrite from the other. Maximal density of sodium conductance in the soma was 800 pS/μm^2, while in the axon it was 10 times higher, 8000 pS/μm^2, and in the dendrite 40 times lower, 20 pS/μm^2 (Yu et al., 2008). Since this model ignores morphological features of real axons—the presence of a hillock at the origin of the AIS and extended length of the axon beyond the initial segment, we have also tested this model but with a more realistic axonal geometry: with the axon hillock, several myelinated segments and nodes, and an unmyelinated terminal. Sodium channel density in the hillock was set 4000 pS/μm^2, which is five times higher than in the soma, and 50% of the AIS density. Other settings remained the same.

In all models, APs were evoked by depolarizing current steps in the soma. In all models, APs were initiated in the distal portion of the initial segment, 30–50 μm from the soma, and backpropagate to the soma, in accordance with experimental results (Stuart et al., 1997a; Palmer and Stuart, 2006).

For quantification of the AP onset dynamics, we have used a recently introduced quantitative criterion: the ratio of the error of the exponential fit to the error of piecewise linear fit for the AP onset in the phase plot (the ratio of fit errors, Volgushev et al., 2008). Data analysis was performed using custom-written programs in MATLAB (V7.1, R14, ©1994–2005 The MathWorks, Inc.) environment. Data are presented as mean$\pm$SD.

RESULTS

AP backpropagation does not necessarily lead to rapid onset dynamics of AP in the soma

To study the AP onset dynamics in the soma of cortical neurons, we started with a model having a simple dendritic tree but a realistic structure of the initial portion of the axon (Fig. 1A). In the model, the axon included a 10 μm hillock, tapering from 4 to 1.2 μm; proximal and distal initial segments (AIS), each 20 μm long and 1.2 μm in diameter, followed by 10 myelinated sections (each 98 μm long, 1.2 μm in diameter) separated by the nodes of Ranvier (2 μm long, 1.08 μm in diameter), and a non-myelinated terminal (100 μm long, tapering from 1.2 to 0.1 μm). We started our

analysis with the distribution of voltage-gated sodium channels over the cell membrane and their properties matching as close as possible the available direct experimental data (Stuart and Sakmann, 1994; Colbert and Pan, 2002; Baranauskas and Martina, 2006, patch clamp data from Kole et al., 2008). The peak sodium conductance gNa in the soma was 100 pS/μm^2, which corresponds to the high end of the values measured in the soma of cortical neurons in cell-attached or inside out patch configuration (Stuart and Sakmann, 1994; Kole et al., 2008; Hu et al., 2009). These studies reported densities of ~30–80 pS/μm^2 (Stuart and Sakmann, 1994; Kole et al., 2008; Hu et al., 2009). Baranauskas and Martina (2006) found in acutely dissociated cells higher current densities corresponding to ~500 pS/μm^2. However, in the models that claimed to reproduce the fast AP onset dynamics (Yu et al., 2008), a much higher value of 800 pS/μm^2 was used. Thus, we opted for a conservatively high value of sodium current in the soma for the main simulations (100 pS/μm^2) and have also tested models with higher densities (300, and 900 pS/μm^2) to make sure that the whole possible range is covered. Direct measurements made in the layer 5 neocortical neurons showed that the density of sodium channels in the AIS was about 2.5–5 times higher than in the soma (Fig. 2d in Colbert and Pan, 2002, and Fig. 4a in Kole et al., 2008), the increase occurring gradually over about 10–15 μm from the soma (Fig. 1d in Kole et al., 2008; Lorincz and Nusser, 2008; Hu et al., 2009). To account for these data in the model, the maximal sodium conductance in the AIS was at least three times higher than in the soma and the maximal sodium conductance in the axon hillock was 50% of the AIS value. This ratio of 3 of the AIS to soma sodium channel densities was the lowest used in our study. Since other estimates suggested a higher density of sodium channels in the AIS (10–50 times of the somatic, e.g. Yu et al., 2008; Kole et al., 2008; Hu et al., 2009), we gradually varied the ratio of sodium channel densities in the AIS to the soma from 3 to 900-fold (or 90,000 pS/μm^2), which is well above any available estimate. In addition, sodium channels in the AIS activated at about 7–15 mV less depolarized membrane potentials than channels in the soma (Colbert and Pan, 2002; Kole et al., 2008; Schmidt-Hieber et al., 2008b; Hu et al., 2009). To account for these data in the model, the activation curve of the AIS sodium currents was shifted by 8 mV towards more hyperpolarized values.

With these parameters, the model reproduced the experimentally observed sequence of events during an AP generation in response to the injection of depolarizing current into the soma: the initiation of an AP in the distal AIS, its propagation from there in both directions, orthodromically down the axon and antidromically into the soma and dendrites, followed by generation of the somatic AP (Stuart et al., 1997a; Palmer and Stuart, 2006). This pattern of AP initiation and backpropagation, illustrated in Fig. 1 A for a model with a low, three-fold AIS/soma ratio of sodium channel densities, was also reproduced in all our simulations, including those with higher densities of sodium channels in the AIS.

Phase plots of APs generated by this model at the initiation site and in the soma show that the AP in the soma has a smooth, slow onset with the onset dynamics only slightly faster than the onset of AP at the initiation site in the distal AIS (Fig. 1B, C). These results demonstrate that distal initiation and backpropagation of an AP does not necessarily lead to the sharp AP onset dynamics in the soma.

Since the goal of this study is to identify the range of parameters that reproduce the rapid AP onset in the models employing the HH-type sodium channel, we need a valid measure for quantification of the AP onset dynamics. Here we used a recently introduced quantitative measure–the ratio of errors of an exponential fit to a piecewise linear fit to the initial AP portion in the dV/dt versus V phase plot (the ratio of fit errors, Volgushev et al., 2008). Previous work has shown that for cortical neurons, the ratio of fit errors was usually $>$6, and in all but one cell $>$3 while for smoothly rising APs in snail neurons the ratio of fit errors was around 1 or lower (Volgushev et al., 2008). Therefore, we will call the AP onset smooth if the ratio of fit errors is below 1 and steep if it is $>$3.

Fig. 2A1–C1 illustrates the results of quantification of the onset dynamics of a somatic AP simulated with the same model as in Fig. 1 but with the density of sodium channels in the AIS five times higher than in the soma. A hump at the beginning of the phase plot in Fig. 2B1 is due to the invasion of the distally initiated AP into the soma. The AP onset in the soma is smooth. In the zoomed in initial portion of the phase plot (Fig. 2C1, black), the model AP trace covers the exponential fit (magenta) almost completely while the piecewise linear fit (cyan) deviates substantially from the model AP trace and remains visible. Thus, the exponential fit to this AP onset is by far better than the piecewise linear fit and the ratio of fit errors is low (0.022). For comparison, an example AP recorded in a neuron in a rat neocortical slice is shown in Fig. 2A2–C2. The AP has a sharp, step-like onset and the piecewise linear fit (Fig. 2C2, cyan) is almost completely covered by the trace of the recorded AP (black) while the exponential fit (magenta) clearly deviates from the recorded trace. Thus, the piecewise linear function provides a far better fit to the data than the exponential function. For this AP, the ratio of fit errors was high (10.5, Fig. 2C2).

In this work we refrained from using as a measure of the AP onset dynamics the “rapidness” that was used in previous work. The “rapidness” was originally defined as a slope of an AP during the onset measured in the dV/dt versus V phase plot at 10 mV/ms (Naundorf et al., 2006), but measured at higher levels in a later paper (Yu et al., 2008). A problem is that, for APs with a smooth onset, the “rapidness” value depends strongly on the level at which it is measured. For the AP illustrated in Fig. 2A1–D1 the onset of which is well described by an exponential function, shifting the measurement point from 10 to 30 mV/ms increases the “rapidness” value by more than 2.5 times, from 3.4 to 8.8 s^{-1} (Fig. 2D1). This effect was consistently reproduced in a variety of models with HH kinetics of sodium channels (Fig. 2F, red, magenta and gray sym-

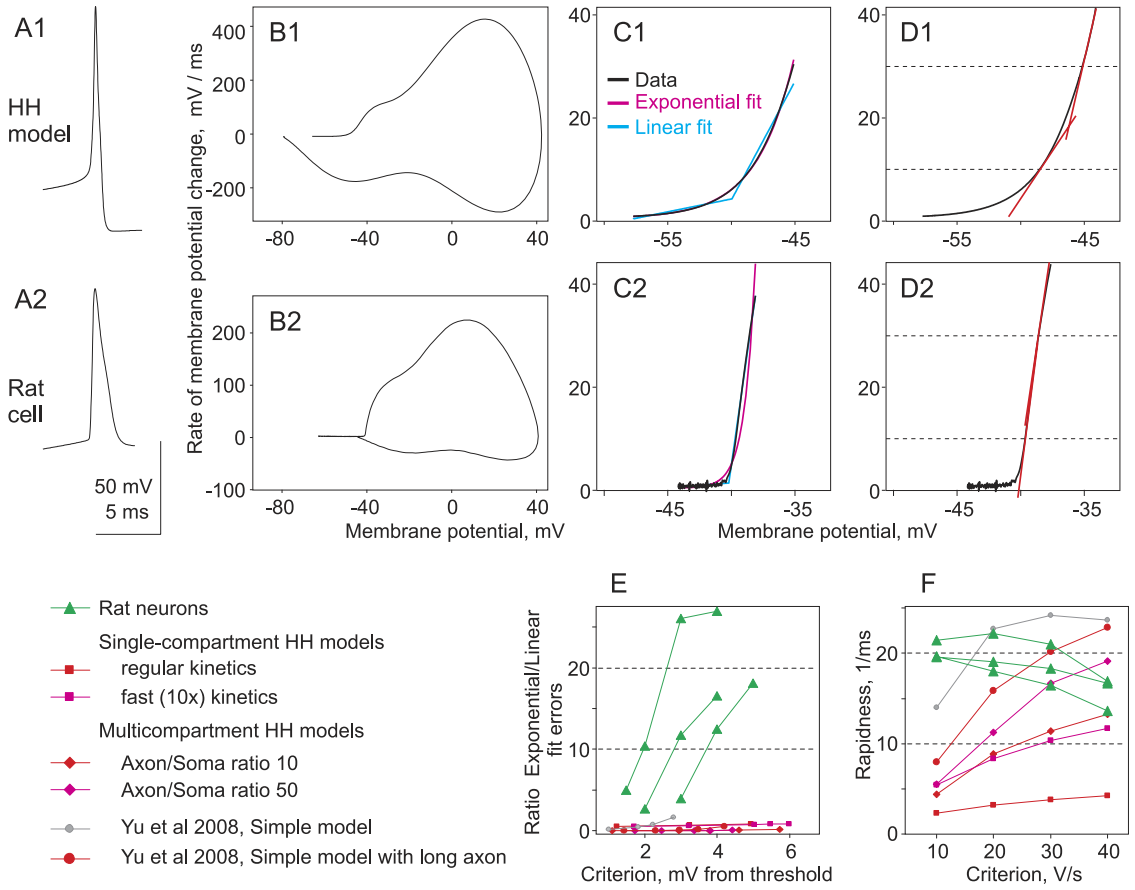

Fig. 2. Quantification of AP onset dynamics: Comparison of two methods. APs simulated with a Hodgkin–Huxley type model (AIS/soma ratio 5) and an AP recorded in a representative neuron in rat neocortex slice. In this and all subsequent figures, APs recorded or simulated in the soma are shown. (A1, A2) AP waveforms. (B1, B2) Phase plots of APs from (A). (C1, C2) Initial portion of APs in phase plot at expanded scale, with exponential (magenta) and piecewise linear (cyan) fits. In this and other figures of this type the AP trace simulated with the model (or recorded in a neuron) is plotted atop of the fitting curves. Thus, better fit is covered more completely by the AP trace. Ratio of errors of exponential to linear fits were 0.022 for the HH model and 10.5 for the Rat cell. (D1, D2) Initial portion of APs in phase plot at expanded scale, with tangential lines at 10 and 30 mV/ms. Note that with higher criterion, the steepness of the tangential slope, "rapidness," increases for the simulated AP, but not for the recorded AP. (E, F) Dependence of the quantitative measures of AP onset dynamics, ratio of the errors of exponential to piecewise linear fits (E) and rapidness (F) on the criterion used for their calculation. Results for APs recorded in three neocortical neurons (green, triangles) and simulated with different models (red and grey). Note that the ratio of exponential/linear fit errors clearly differentiate between a stepwise onset dynamics of recorded APs and smooth onset dynamics of simulated APs. In contrast, the rapidness captures the difference between the recorded and simulated APs only when measured at the very beginning of APs (10 mV/ms), but not when measured at higher dV/dt values.

bols). In contrast, the "rapidness" of APs recorded in rat neocortical neurons does not show such a dependence on the dV/dt value at which the measurement is made and changes little or even decreases slightly when the slope measurement point is shifted from 10 to 30 mV/ms (19.6 vs. 18.3 s^{-1} in Fig. 2D2; more data are shown in Fig. 2F, green triangles). As a result, for the "rapidness" measured at 10 mV/ms, a clear and consistent difference is found between the smooth onset in simulated APs and the steep onset of recorded APs. However, if the measurement point is shifted to 20 mV/ms or higher, this difference between a smooth and a step-like AP onset becomes much less pronounced. If the "rapidness" is measured at ≥30 mV/ms, the difference almost disappears (Fig. 2F). This effect may explain in part why (Yu et al., 2008) conclude that the AP onset is steep even in the models which actually produce AP with an onset much smoother than in neurons. Note that the "simple model" of Yu et al. (2008), does have a steep onset that is captured by the rapidness measure at 10 mV/ms (Fig. 2F, gray line). This model is discussed below in the results section.

The AP onset measure employed in the present study, the ratio of errors of exponential over piecewise linear fits, has several advantages over the measure of rapidness. The ratio of fit errors is calculated on the basis of many data points covering the interval just before the AP onset and the initial portion of the AP slope. Thus, the ratio of fit errors characterizes the dynamics of the AP onset as such. The rapidness is measured using only two or three data points on the AP slope, after the threshold had been exceeded, and thus actually measures the speed of an already started regenerative irreversible process. Although the ratio method is more reliable in our hands, it has a drawback of its own: it is affected by the recording noise,

which is not present in model traces. The presence of noise in a trace increases the errors of both fits by a similar amount, and thus biases the ratio of fit errors towards 1. However, since in real central neurons the ratio of fit errors was well above 1 but in most simulations <1, such a bias would tend to decrease the actual difference. Therefore, this quantification method provides a conservative estimate of the difference between the onset of the recorded and simulated APs. In contrast to the "rapidness," the ratio of fit errors consistently captures the difference between the smooth and the step-like onset dynamics (Fig. 2E). Although the exact value of the ratio of fit errors does depend on the portion of the AP onset chosen for the fits, the difference between the APs with a step-like onset (green triangles in Fig. 2E) and the APs with a smooth onset (red, magenta and gray symbols in Fig. 2E) remains significant over the whole range of settings. Thus, in this paper, we used the ratio of fit errors to quantify and compare the onset dynamics of APs in different models and in neurons.

In our simulations we employed either the canonical Hodgkin–Huxley model of sodium channels in which a channel has to pass two intermediate closed states before it can open thus causing a delay (Hodgkin and Huxley, 1952a,b; Hodgkin et al., 1952) or a modified version of the HH-model in which a channel rapidly passes a single closed state before reaching an open state thus reducing dramatically the delay before opening (Baranauskas and Martina, 2006; BM-model). Although a large number of variations of the canonical Hodgkin–Huxley model can be found in literature, most of these variations share very similar activation kinetics, a crucial parameter in our study (Supplementary Fig. S1). A notable exception is the Engel and Jonas (2005) model based on the recordings from presynaptic mossy fiber boutons. The activation kinetics of sodium channels in the Engel and Jonas (2005) model is comparable to BM model (Supplementary Fig. S1A, B), however APs simulated with Engel and Jonas model have slower AP onset kinetics (Supplementary Fig. S1D). Thus, the HH and BM models used here should cover the whole range of possible sodium channel kinetics reported so far. We studied the influence of the following parameters on the AP onset dynamics: (i) distribution of sodium channels in the AIS and soma–the ratio of channel density in the AIS/soma, and the absolute value of maximal sodium current (gNa) in the soma; (ii) the presence of persistent sodium current $I_{Na\text{-}pers}$, and the density of the rapid delayed rectifier current I_{Kv}; (iii) passive cell properties: the cytoplasmic resistance Ra and the membrane leak conductance, (iv) the axon geometry: the diameter and the length of the AIS, and (v) temperature. In addition, we measured the ratio of fit errors for several published models with realistic, detailed neuron morphology models ((Mainen et al., 1995; Mainen and Sejnowski, 1996) available at SenseLab's ModelDB database, URL: http://senselab.med.yale.edu/senselab/modeldb). Parameters of the models used here and the ranges of parameters tested are summarized in Table 1.

Dependence of the onset dynamics of somatic APs on the density of voltage-gated sodium channels in the AIS and soma

We varied sodium channel density in the AIS from 3 to 900 times higher than in the soma, and used three different values of the maximal sodium conductance in the soma: 100, 300 and 900 pS/μm^2 (10, 30 and 90 mS/cm^2). Altogether our models covered the range of gNa in the AIS from 300 to 270,000 pS/μm^2 (Table 1). All simulations of this series were made with our basic model neuron morphology, exact same as in Fig. 1.

Fig. 3A shows APs generated with models in which the density of HH sodium channels in the AIS was 10, 50 and 300 times higher than in the soma while the somatic channel density was kept constant at 100 pS/μm^2. A comparison of the dV/dt against V phase plots of the simulated APs (Fig. 3A and zoom in of the initial portion in Fig. 3B) reveals several effects of the increasing sodium channel density in the AIS on the AP properties. The apparent threshold of the somatic AP decreases as indicated by the leftward shift of the AP origin in the phase plot. The AP maximal amplitude and the maximal rate of membrane potential depolarization increase. Finally, the steepness of the AP initial portion in the phase plot increases. However, the zoomed in initial portion of the somatic AP phase plot (Fig. 3B) shows that the dynamics remains smooth, exponential-like. The ratio of fit errors is low for APs simulated with all three sodium channel densities in the AIS (0.033, 0.078 and 0.07).

Steeper AP onsets were obtained with the BM model that included high sodium channel densities. Fig. 3C, D shows APs simulated by the models employing BM sodium channels (gNa in the soma was roughly equivalent to 100 pS/μm^2=10 mS/cm^2, same as in the above HH models). The density of sodium channels in the AIS was again 10, 50 and 300 times higher than in the soma. The effects of increasing the BM sodium channel density in the AIS were similar to those in the models employing HH sodium channels: the apparent AP threshold in the soma decreases and the AP maximal amplitude and the maximal rate of the membrane potential depolarization increase (Fig. 3C). The AP onset was steeper in models equipped with BM sodium channels than in the models with canonical HH sodium channels (compare Fig. 3B, D). Nevertheless, the expanded initial portion of APs in Fig. 3D shows that, for sodium channel densities in the AIS that were 10 or 50 times higher than in the soma, the AP onset dynamics remained smooth, exponential-like. For these APs, the ratios of fit errors were 0.56 and 0.38, respectively. Only for the density of sodium channels in the AIS, 300 times higher than in the soma, the AP onset dynamics became steeper. In this latter case, a piecewise linear function provided slightly better fit to the onset of the simulated AP than an exponential function (the ratio of fit errors 1.6).

The summary of these simulations is presented as a plot of the ratio of fit errors against the ratio of AIS/soma sodium channel densities (Fig. 3E, simulations employing HH sodium channels are shown in purple triangles, and

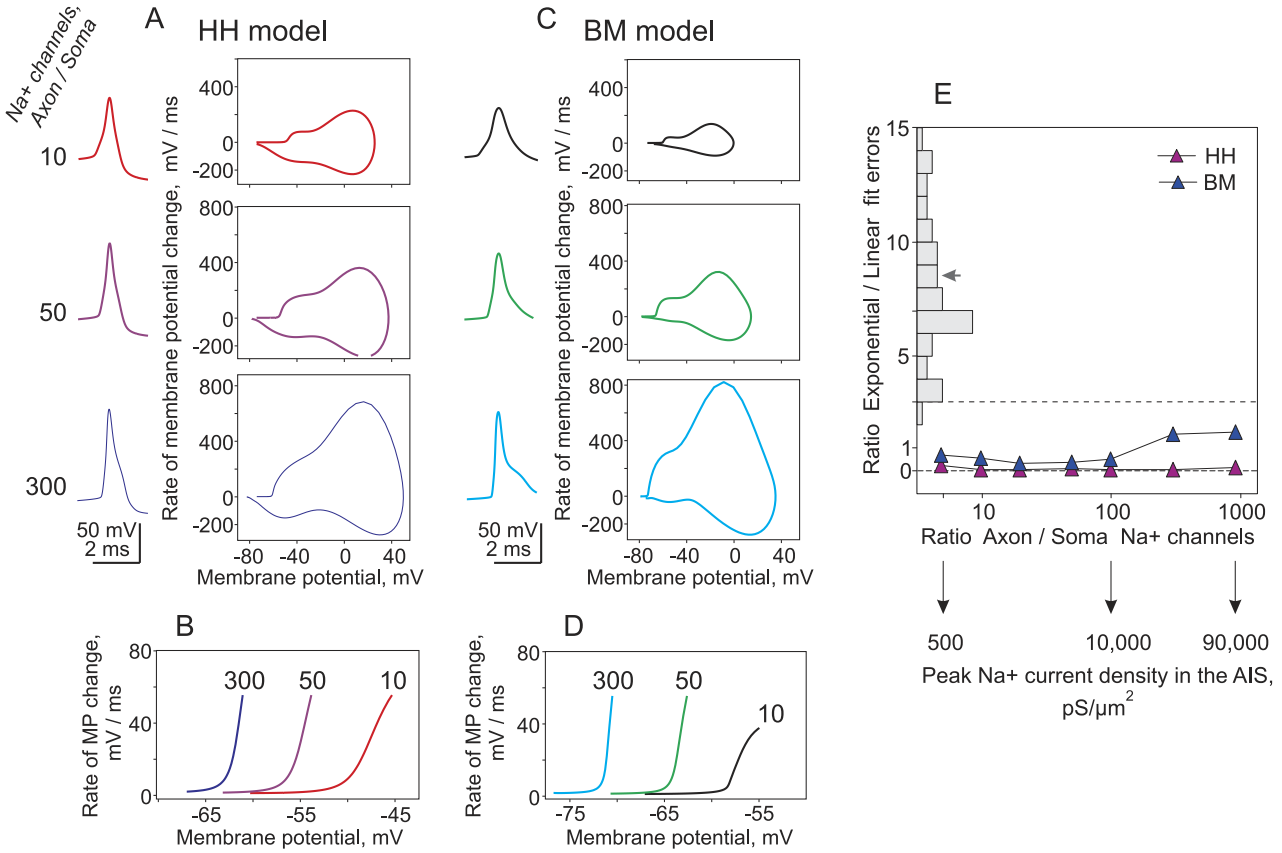

Fig. 3. Dependence of AP onset dynamics on the AIS/soma ratio of sodium channel density. (A, B) AP waveforms, phase plots and zoom in of the initial portion of the phase plots for the HH model with the density of sodium channels in the AIS 10, 50 and 300 times higher than in the soma. The ratios of errors of exponential to piecewise linear fits for these APs were: 0.033, 0.078, 0.07. (C, D) Data for the model with BM type sodium channels, same representation as in (A, B). The ratios of fit errors were: 0.56, 0.38, 0.54. The neuron model morphology in all simulations was the same as in Fig. 1. Numbers on the left show AIS/soma ratios of channel density for both HH and BM models. (E) Dependence of the ratio of fit errors on the ratio of AIS/soma channel density for the models with HH and BM type sodium channels. For comparison, in this and all further plots of that kind, distribution of the ratios of fit errors for 49 rat neocortical neurons (data from Volgushev et al., 2008) is shown in light gray on the left-hand side. The length of each bar in the distribution is proportional to the number of neurons in which APs had the ratio of fit errors corresponding to the bar location on the vertical scale. Out-of-scale values for three neurons with error ratios between 15 and 22 are not shown. Black arrow shows mean value of the ratio of fit errors for that sample of rat neocortical neurons (8.46±3.87, n=49). Horizontal interrupted line is drawn at the ratio of fit errors=3. In this sample, APs in only 1 out of 49 neurons had the ratio of fit errors below 3. For interpretation of the references to color in this figure legend, the reader is referred to the Web version of this article.

simulations employing BM sodium channels are represented by blue triangles). For comparison of the simulated APs to those recorded, the distribution of the ratios of fit errors obtained for 49 neurons recorded in slices from the rat neocortex is shown on the left vertical axis (data from Volgushev et al., 2008). Fig. 3E demonstrates that, for the passive properties and neuron geometry used in these simulations, the ratio of fit errors is usually well below the range found in neurons. The exception is the ratio of fit error of 1.6 and 1.7 attained in simulations employing BM sodium channel model with the density of sodium channels in the AIS 300 and 900 times higher than in the soma (corresponding to ~30,000 and 90,000 pS/μm^2). However, even these values of the ratio of fit errors are only approaching the low end of the range found in neurons (Volgushev et al., 2008).

To test how changes in the overall sodium channel density affect the onset dynamics of APs, we increased the gNa of HH sodium channels in the soma from 100 to 300 pS/μm^2 and 900 pS/μm^2 while varying the ratio of the AIS/soma sodium channel densities from 3 to 300. In all these tests, just increasing the density of HH-type sodium channels in the soma had negligible effects on the ratio of fit errors (Supplementary Fig. S2). In all these tests the ratio of errors did not reach 1 (0.82 for the highest gNa tested, 900 pS/μm^2 in the soma and 270,000 pS/μm^2 in the AIS). The fact that increasing sodium channel density in the soma did not lead to a sharper onset of somatic APs is consistent with the conclusion reached by Yu and colleagues (Yu et al., 2008) that in the invasion scenario the somatic AP onset dynamics is determined by the properties of the current (called Iprop, Yu et al., 2008) that invades the soma before the generation of local AP in the soma. This invasion component caused by Iprop can be revealed by elimination of sodium channels from all compartments but the AIS (Yu et al., 2008). Simulations employing this method of Iprop isolation confirmed that only the AIS but not somatic sodium channels determine

the AP onset in the invasion scenario (Supplementary Fig. S3).

Thus, for our neuron model geometry and standard axon passive properties, we failed to obtain a rapid AP onset in the soma even with the extremely high gNa in the AIS (up to 270,000 pS/μm^2). Here it is important to note that, in simulations described so far, we used very few voltage dependent currents. However, in the axons several subthreshold voltage dependent currents are present (Astman et al., 2006; Kole et al., 2007) and these currents potentially may change the Iprop and thus the onset dynamic of somatic AP. Therefore, next we tested the effects of subthreshold currents on the somatic AP onset dynamics.

Dependence of the onset dynamics of somatic APs on fast potassium currents and persistent sodium current

The presence of fast potassium channels at high density in the AIS (10,000 pS/μm^2, 10 times higher than in our basic model) leads to a decreased AP duration in the AIS (Kole et al., 2007), accompanied by an increased separation between the initial hump and the main loop in the AP phase plot (arrows in Fig. 4B1). Fig. 4B1 shows this effect for a model employing BM sodium channels, with their density in the AIS 100 times higher than in the soma. However, this change in the shape of the AP phase plot did not lead to a detectable change of the AP onset dynamics for all tested sodium channel densities in the AIS (Fig. 4D, light blue diamond symbols).

Another candidate current that may influence the AP onset dynamics is the persistent sodium current that is present in the AIS of neocortical neurons (Astman et al., 2006). To test whether the presence of this current can influence the AP onset dynamics, we made simulations with a model that included persistent sodium current with peak amplitude of 5% of the maximal amplitude of the fast sodium current in axon hillock and initial segment (Astman et al., 2006). Similarly to the fast potassium current, the presence of the persistent sodium current had little effect on the AP onset dynamics (Fig. 4A2, B2, C and green square symbols in 4D). The absence of effects could not be attributed to the voltage dependence of these two conductances because variations of the activation midpoints over a wide range of voltages did not have any significant effect (data not shown).

These two series of simulation experiments show that the presence of high density of potassium channels in the

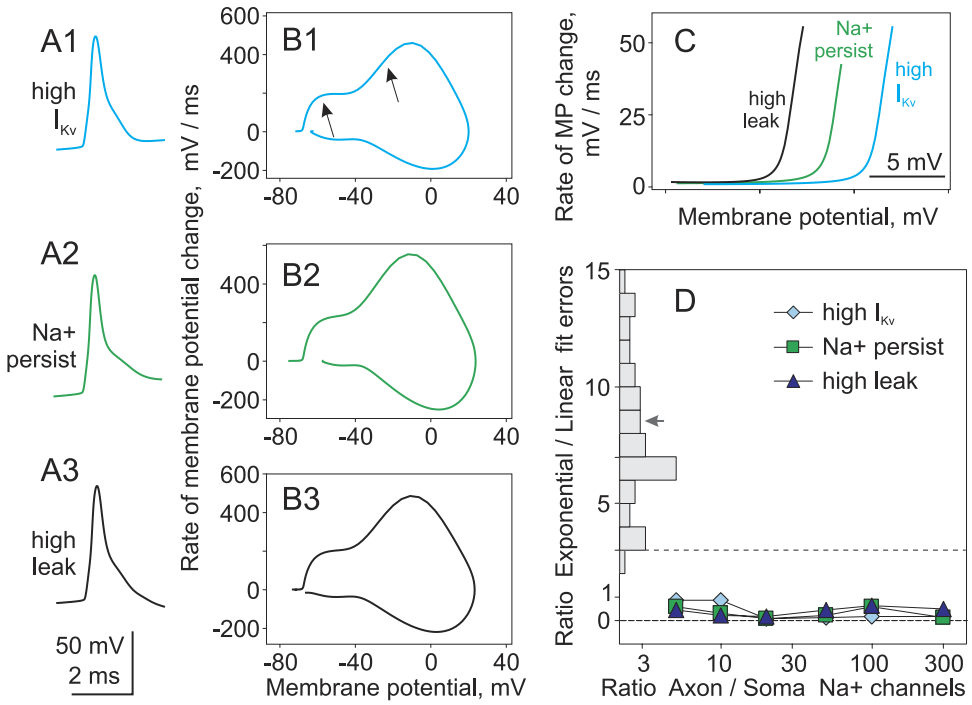

Fig. 4. Influence of fast potassium conductance, persistent sodium current and leak conductance on AP onset dynamics. Onset dynamics of APs simulated with models with high density of fast potassium channels in the axon initial segment (A1, B1), persistent sodium current (A2, B2) and high membrane leak conductance (A3, B3). (A, B) AP waveforms and phase plots. (C) Zoom in of the initial portions of the phase plots from (B). Note that plots in (C) are shifted along the X-axes to show onset of all three APs, which had similar threshold and would coincide almost completely without a shift. Basic model with BM type sodium channels was modified as following: high density of fast potassium current in the axon initial segment (A1, B1, I_{kv}, 30 times higher than in the basic model); persistent sodium current with peak amplitude 5% of the fast sodium current in the axon hillock and initial segment (A2, B2); and high membrane leak conductance (A3, B3, ~16 times higher than in the basic model). In all three examples in (A, B), fast sodium channels had BM type kinetics, and their density in the AIS was 100 times higher than in the soma. Ratios of fit errors were: 0.17 for A1, B1; 0.58 for A2, B2 and 0.66 for A3, B3. (D) Dependence of the ratio of fit errors on the ratio between AIS/soma sodium channel density for the three models. Distribution of the ratio of fit errors in rat neocortical neurons along the ordinate and the mean of experimental data (arrowhead) as in Fig. 3E. For interpretation of the references to color in this figure legend, the reader is referred to the Web version of this article.

AIS or the presence of persistent sodium current do not change appreciably the onset dynamics of somatic AP in the invasion scenario. These results also show that, for model parameters used here, Iprop is faster than the kinetics of any channels located in the soma or along the way of its propagation through the AIS. Since the time-course of Iprop can be modified during the travel along the axon by the currents flowing through already open channels, next we tested how passive membrane properties and parameters determining the axon cable properties influence the AP onset dynamics.

Dependence of the onset dynamics of somatic APs on passive properties: membrane leak conductance and cytoplasmic resistance

In the above simulations, we used commonly accepted values of passive cell properties such as membrane leak conductance (0.000 02 S/cm^2=0.2 pS/μm^2) and the cytoplasmic resistance (150 Ohm×cm). The same or similar values of these parameters were used in previous models of neocortical neurons (e.g. in Mainen et al., 1995; Mainen and Sejnowski, 1996; Destexhe and Pare, 1999; Destexhe et al., 2001; Kole et al., 2008; Yu et al., 2008). However, these values are largely indirectly derived from the experimental data and imprecision of their estimations could be a potential reason for the differences in the AP onset dynamics between neurons and our simulations.

To test the effects of large leak conductance in the soma on the dynamics of the AP onset, we increased the membrane leak conductance ~16 times, from 0.000 02 to 0.000 33 S/cm^2 (from 0.2 to 3.3 pS/μm^2). Consequently, the conductance load of the soma and dendritic arbor increased from ~1.7 to ~28 nS, a value similar to the one used in a recent model (Yu et al., 2008). This ~16-fold increase in the total conductance of the somato–dendritic compartment lead to only minor changes of the AP shape, and did not make the AP onset dynamics much faster (Fig. 4A3, B3, C). Within the range of the AIS sodium channel densities tested, 3 to 300 times higher than in the soma (up to 90,000 pS/μm^2), the onset dynamics of the simulated APs remained smooth, better fitted by an exponential than by a piecewise linear function (Fig. 4D, triangles).

To test how the cytoplasmic resistance influences the shape and onset dynamics of the somatic APs, we varied this parameter between the values three times lower and three times higher than in our standard model (150 Ohm×cm), thus covering the range from 50 to 450 Ohm×cm. For a neuron model with low axial resistance (50 Ohm×cm), the simulated APs displayed a substantially increased amplitude of the initial hump in the phase plots, reflecting the increased flow of current from the axon to the soma (Fig. 5A, compare to Fig. 3). However, this increased axonal contribution to the somatic AP shape did not lead to the sharper onset dynamics. For all tested sodium channel densities in the AIS, the fit error ratio was lower than in the models with standard axial resistance of 150 Ohm×cm (Fig. 5F).

Increasing the cytoplasmic resistance to 450 Ohm×cm had profound effects on the shape and onset dynamics of the simulated APs. In the waveforms of APs produced by these models, an initial shoulder on the rising slope of APs becomes apparent (arrows in Fig. 5C). This shoulder cor-

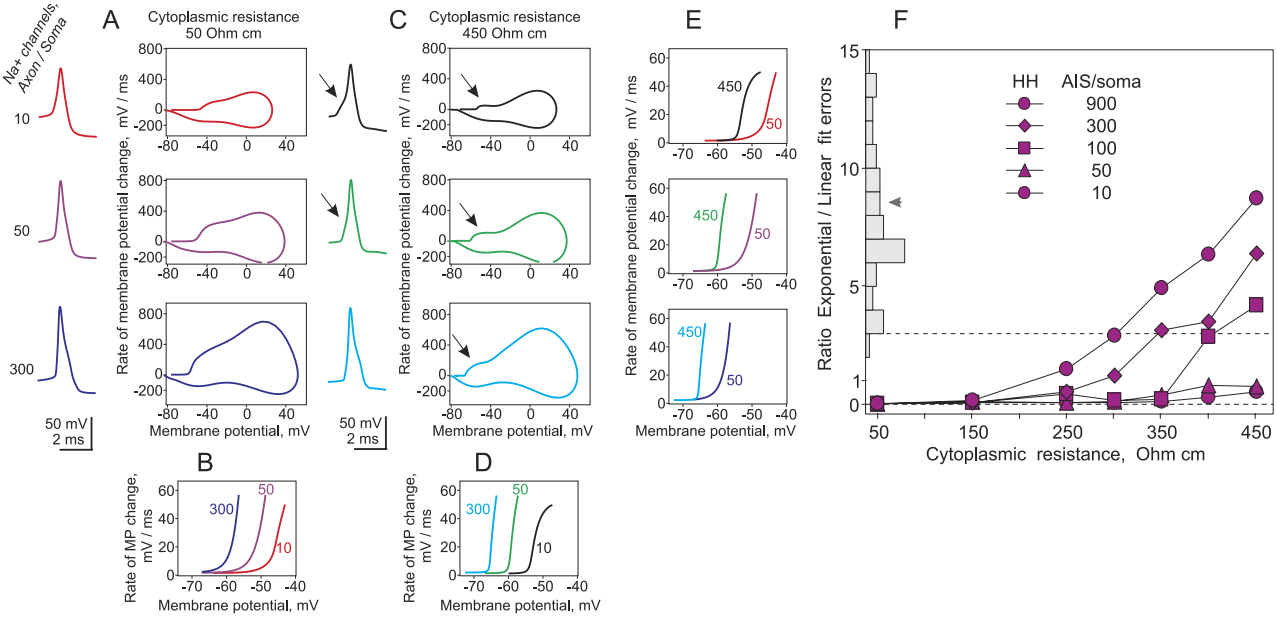

Fig. 5. Dependence of the AP onset dynamics on the cytoplasmic resistance. (A–E) AP waveforms, phase plots and zoom in of the initial portion of the phase plots for the HH model with cytoplasmic resistance 50 Ohm×cm (A) and 450 Ohm×cm (C) and density of sodium channels in the AIS 10, 50 and 300 times higher than in the soma. Initial portions of the phase plots are shown at expanded scale for respective columns (B, D) or rows (E). Color code is the same in (A–E). (F) Dependence of the ratio of fit errors on the axial resistance for HH models with different ratios of the AIS/soma sodium channel density, as indicated. Distribution of the ratio of fit errors in rat neocortical neurons along the ordinate and the mean of experimental data (arrowhead) as in Fig. 3E. For interpretation of the references to color in this figure legend, the reader is referred to the Web version of this article.

responds to the invasion component, which is clearly distinguishable from the somatic AP (Fig. 5C). A combination of high cytoplasmic resistance (Rax ≥~300 Ohm×cm) with very high densities of sodium channels in the AIS (100 to 900 times higher than in the soma, or ~10,000 pS/μm^2 for Rax ~400–450 Ohm×cm, and ≥~30,000 pS/μm^2 for Rax ≥~300 Ohm×cm) allowed to achieve the sharp onset of the invasion component in the soma (Fig. 5D–F). The ratios of fit errors for APs generated by these models were close to or above 3 (Fig. 5F). The same result was obtained in simulations employing BM model of sodium channels (data not shown).

Dependence of the onset dynamics of somatic APs on the geometry of the axon initial segment

Axon geometry is another factor, which may change the Iprop and thus the onset dynamics of the somatic AP. Indeed, it has been shown that the onset dynamics of Iprop becomes faster after traveling 300–400 μm along a thin axon (Yu et al., 2008). To test the effects of axon morphology on the onset dynamics of somatic APs, we varied the AIS diameter and length. Morphological data provide reliable information on the dimensions of the AIS: for layer 5 pyramidal cells it is approximately 40 μm long and 1–3 μm in diameter, for example (Sloper and Powell, 1979; Palmer and Stuart, 2006; Kole et al., 2007). The AIS size in our basic model (40 μm long, 1.2 μm diameter) was well within these constraints. In the following series of simulations, we analyzed APs in the models in which either the AIS diameter varied from 0.8 to 1.8 μm or the AIS length increased from 40 to 70 μm.

The AIS diameter strongly influenced the AP onset dynamics. The models with BM sodium channels that combined the thin AIS (0.8 μm in diameter instead of 1.2 μm in our basic model), increased cytoplasmic resistance (Rax=250 Ohm×cm instead of 150 Ohm×cm in the basic model) and high sodium channel density in the AIS (100 or more times higher than in the soma, corresponding to ≥~10,000 pS/μm^2) generated APs with a sharp onset dynamics (Fig. 6A, B). For these APs, the ratio of fit errors was ≥3, and thus within the range of the values obtained for the APs recorded in rat neocortical neurons (Fig. 6F, circles and Fig. 6G, diamond symbols). However, in the models with either a larger diameter axon, or a lower density of sodium channels in the AIS, APs had a smooth onset dynamics (Fig. 6F, G). Similar dependence of the AP

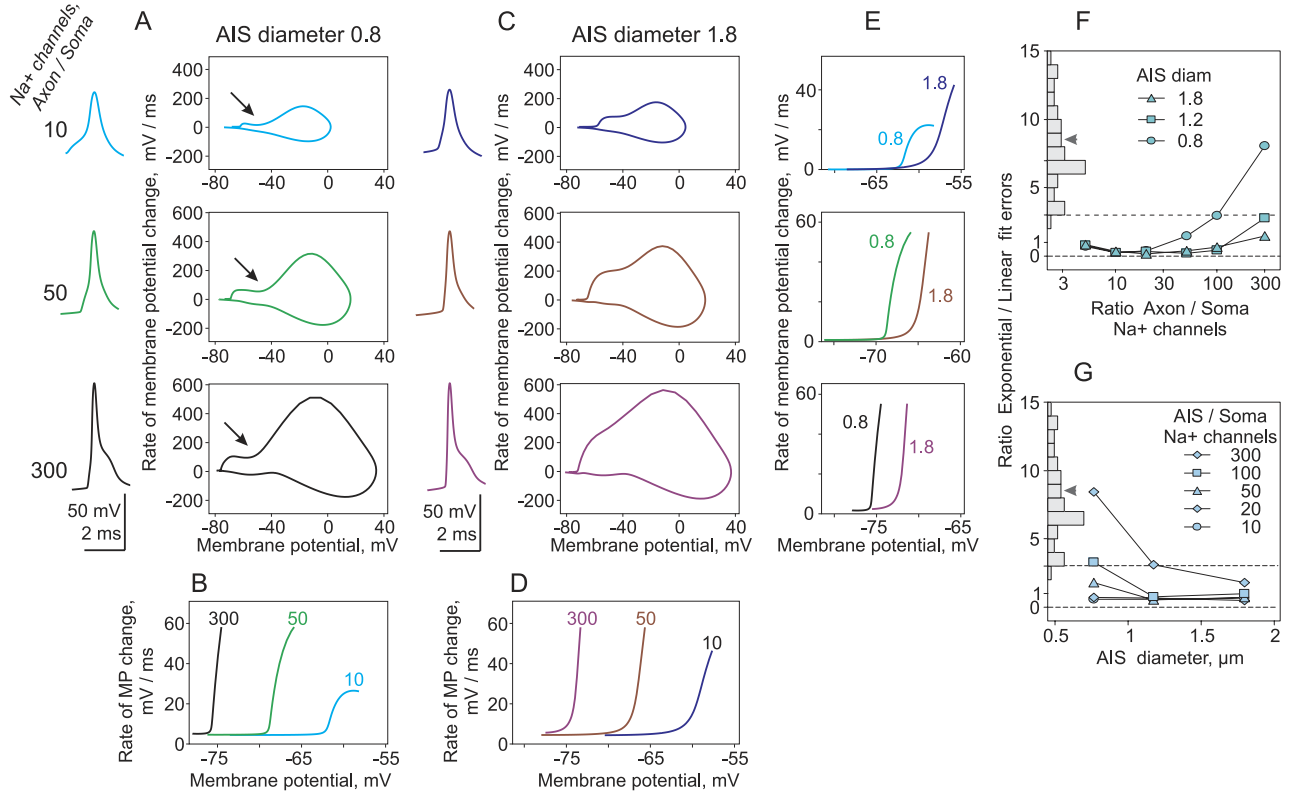

Fig. 6. Dependence of AP onset dynamics on AIS diameter in models with BM sodium channels. (A–E) AP waveforms, phase plots and zoom in of the initial portion of the phase plots in models with BM type sodium channels, having a narrow (A, 0.8 μm diameter) and a wide (C, 1.8 μm diameter) AIS. Sodium channel density in the AIS was 10, 50 and 300 times higher than in the soma, as indicated on the left. Initial portions of the phase plots are shown at expanded scale for respective columns (B, D) or rows (E). Color code is the same in (A–E). (F) Dependence of the ratio of fit errors on the ratio of AIS/soma channel density for three models with axon initial segments with a small (0.8 μm), medium (1.4 μm) and large (1.8 μm) diameter. (G) Dependence of the ratio of fit errors on the axon diameter for the models with different ratios of the AIS/soma sodium channel density, as indicated. Distribution of the ratio of fit errors in rat neocortical neurons along the ordinate and the mean of experimental data (arrowhead) in (F, G) as in Fig. 3E. All models in (A–G) had BM type sodium channels. For interpretation of the references to color in this figure legend, the reader is referred to the Web version of this article.

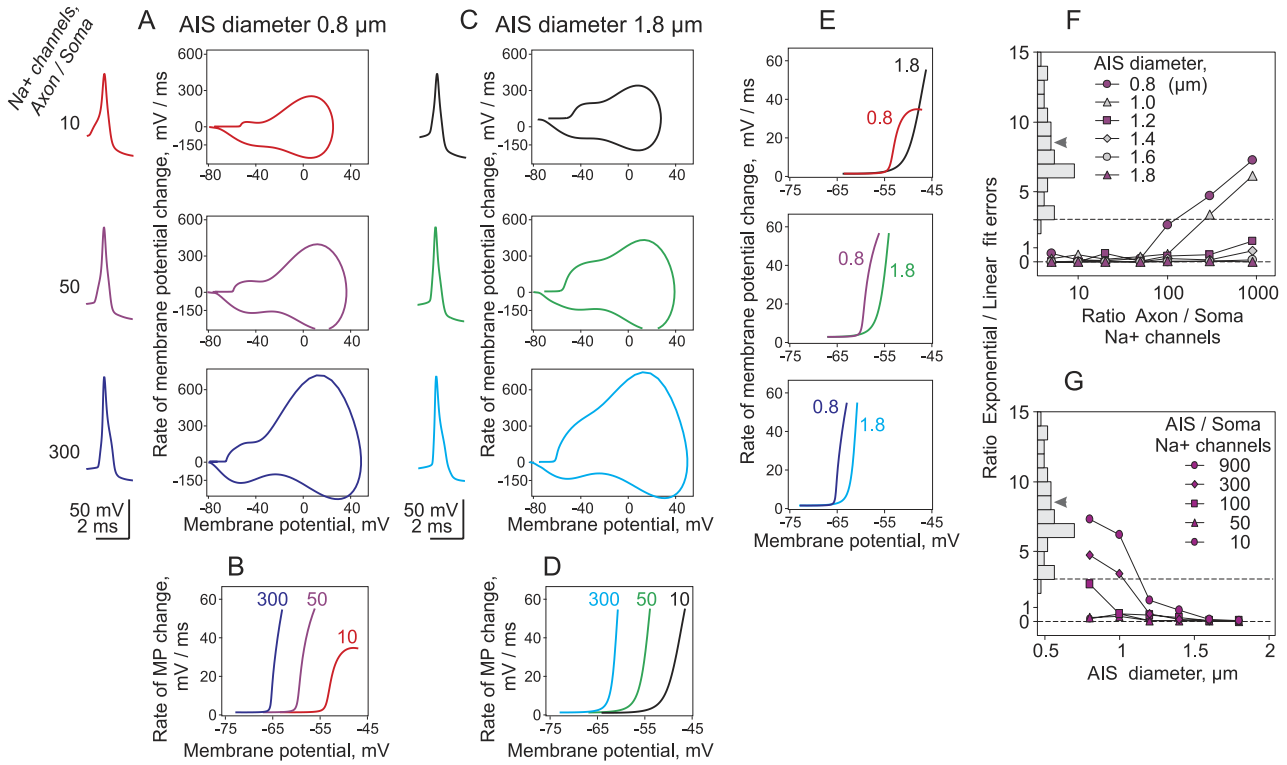

Fig. 7. Dependence of AP onset dynamics on AIS diameter in HH models. (A–E) AP waveforms, phase plots and zoom in of the initial portion of the phase plots in models with HH type sodium channels, having a narrow (A, 0.8 μm diameter) and a wide (C, 1.8 μm diameter) AIS. Sodium channel density in the AIS was 10, 50 and 300 times higher than in the soma, as indicated on the left. Initial portions of the phase plots are shown at expanded scale for respective columns (B, D) or rows (E). Color code is the same in (A–E). (F) Dependence of the ratio of fit errors on the ratio of AIS/soma channel density for six models with different axon initial segment diameters (from 0.8 to 1.8 μm), as indicated. (G) Dependence of the ratio of fit errors on the axon diameter for the models with different ratios of the AIS/soma sodium channel density, as indicated. Distribution of the ratio of fit errors in rat neocortical neurons along the ordinate and the mean of experimental data (arrowhead) in (F, G) as in Fig. 3E. All models in (A–G) had HH type sodium channels. For interpretation of the references to color in this figure legend, the reader is referred to the Web version of this article.

onset dynamics on the AIS diameter was found in models with HH sodium channels (Fig. 7, Rax=250 Ohm×cm). In HH models, the requirements for the density of sodium channels were even higher than for the models with BM sodium channels. To produce APs with a step-like onset, HH models with an AIS diameter 0.8 μm required sodium channel density in the AIS >~100 times higher than in the soma (gNa in the AIS of ≥~10,000 pS/μm^2), and models with 1 μm AIS diameter required sodium channel density in the AIS ≥~300 times higher than in the soma (gNa in the AIS of ≥~30,000 pS/μm^2; Fig. 7F, G). Note that Figs. 6 and 7 illustrate results obtained in models with increased cytoplasmic resistance (Rax=250 Ohm×cm instead of 150 Ohm×cm in the basic model). In models in which cytoplasmic resistance was regular (Rax=150 Ohm×cm) or lower, steep AP onsets were not achieved even with the minimum AIS diameter (0.8 μm) and maximal density of sodium channels (90,000 pS/μm^2) tested (see below, Fig. 10).

In contrast to the AIS diameter, increasing the length of the AIS from 40 to 70 μm had a moderate effect on the shape and onset dynamics of APs. Even with the highest density of HH sodium channels in the AIS (900 times higher than in the soma, 90,000 pS/μm^2) the ratio of fit errors was ~1 in the model with a 70 μm long AIS (Supplementary Fig. S4).

The shape of Iprop may be altered when it travels between compartments with abruptly changing properties, for example from a narrow axon into a large soma with high capacitance and conductance load (Yu et al., 2008). This effect was demonstrated in Yu and colleagues "simple model" consisting of three compartments: a 1 μm thin 50 μm long AIS and a 5 μm thick 3000 μm long dendrite, attached to a 30×20 μm^2 soma from the opposite sides. The density of HH type sodium channels in the AIS was 10 times higher (8000 pS/μm^2) than in the soma. The APs simulated with this model had indeed faster onset than in most other models. With the ratio of fit errors 1.76, the onset dynamics of this AP just approached the lower end of the experimentally measured values (Fig. 8E, brown triangle; see also Supplementary Fig. S5). However, this model does not take into account the presence of the axon hillock, and deviates from the available immunohistochemical data, which show a smooth transition from the high density of sodium channels in the AIS to a lower density in the hillock and soma (Inda et al., 2006; Kole et al., 2008; Lorincz and Nusser, 2008). To test, to which extent the dynamics of AP onset in this model was due to the artificial

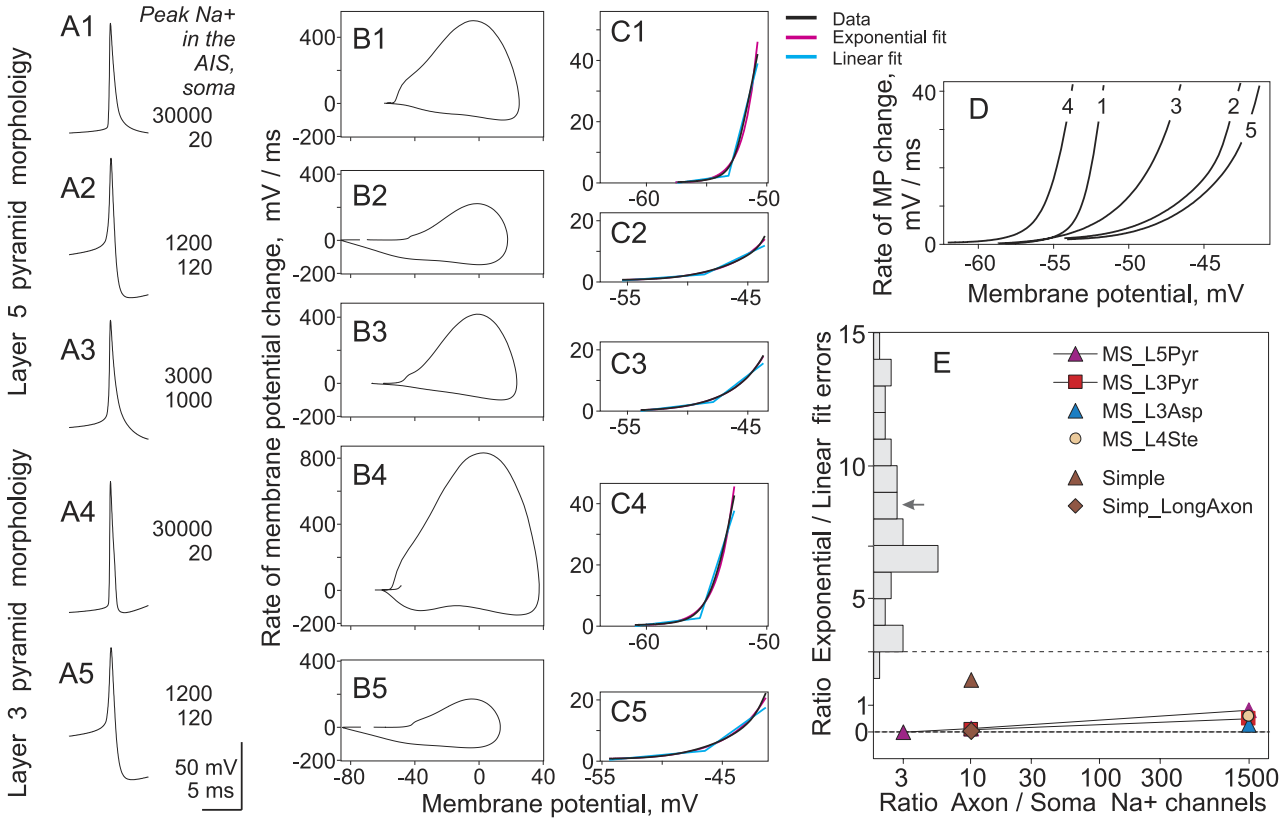

Fig. 8. APs onset dynamics in models with realistic and simplistic morphology. Models with realistic morphology of layer 5 pyramidal neuron (A1–A3), layer 3 pyramidal neuron (A4, A5), layer 3 aspiny cell and layer 4 spiny stellate cell (Mainen et al., 1995; Mainen and Sejnowski, 1996) were downloaded from SenseLab's ModelDB database URL: http://senselab.med.yale.edu/senselab/modeldb. (A–C) AP waveforms, phase plots and zoom in of the initial portion of the phase plots with their exponential and piecewise linear fits in models with realistic morphology. (A1–C1) Model of layer 5 pyramid with original settings (Mainen et al., 1995; Mainen and Sejnowski, 1996) of distribution of conductances and channel kinetics. (A2–C2) Layer 5 pyramid model, but with distribution of sodium and potassium channels as in (Destexhe and Pare, 1999; Destexhe et al., 2001): Maximal sodium conductance in the soma and dendrites 120 pS/μm^2, and 10 times higher in the axon 1200 pS/μm^2. Maximal potassium conductance in the soma and dendrites 100 pS/μm^2 in the axon 1000 pS/μm^2. (A3–C3) Layer 5 pyramid model, but with experimentally reported ratios and kinetics of sodium channels in the axon and soma (Colbert and Pan, 2002; Kole et al., 2008): in the axon initial segment, maximal sodium conductance was three times higher than in the soma (3000 and 1000 pS/μm^2), and its activation curve was shifted by 8 mV towards hyperpolarizing potentials. (A4–C4) Model of layer 3 pyramid with original settings (Mainen et al., 1995; Mainen and Sejnowski, 1996) of distribution of conductances and channel kinetics. (A5–C5) Layer 3 pyramidal neuron, but with distribution of sodium and potassium channels as in (Destexhe and Pare, 1999; Destexhe et al., 2001). In (C1–C5), the ratios of fit errors were: 0.82 in C1; 0.13 in C2; 0.01 in C3; 0.50 in C4; 0.10 in C5. (D) An overlay of initial portions of the phase plots of APs from (A–C). Numbers on the traces correspond to those in (A–C). (E) Ratio of fit errors for APs generated with models with realistic (Mainen et al., 1995; Mainen and Sejnowski, 1996) and simplistic (Yu et al., 2008) morphology, plotted against the ratio of AIS/soma sodium channel densities. Models with realistic morphology of layer 5 pyramidal neuron (MS_L5Pyr), layer 3 pyramidal neuron (MS_L3Pyr), layer 3 aspiny cell (MS_L3Asp) and layer 4 spiny stellate cell (MS_L4Ste) were downloaded from SenseLab's ModelDB database. For layer 3 and layer 5 pyramids, models with original settings (Mainen et al., 1995; Mainen and Sejnowski, 1996) and modified sodium channels densities (according to (Destexhe and Pare, 1999; Destexhe et al., 2001) and (Colbert and Pan, 2002; Kole et al., 2008)) were used. Data points for models with the same morphology are connected with lines. Model with simplistic morphology (brown triangle, "Simple," sodium channel density in the AIS 10 times higher than in the soma, the ratio of fit errors 1.76) consisted of three components: a 30×20 μm^2 soma, a 1 μm thin 50 μm long axon initial segment attached directly to the soma from one side, and a 5 μm thick 3000 μm long dendrite from the other (Yu et al., 2008). In the modification of that model with more realistic axon structure (brown diamond, "Simp_LongAxon," sodium channel density in the AIS 10 times higher than in the soma, the ratio of fit errors 0.1) the axon was extended by adding several myelinated segments, nodes of Ranvier and a thin unmyelinated terminal and characteristic geometry of the axon hillock. Distribution of the ratio of fit errors in rat neocortical neurons along the ordinate and the mean of experimental data (arrowhead) as in Fig. 3E. For interpretation of the references to color in this figure legend, the reader is referred to the Web version of this article.

AIS geometry, we modified it to better match the experimental data by (i) extending the axon beyond the initial segment by adding several myelinated segments, the nodes of Ranvier and a thin unmyelinated terminal, (ii) reproducing characteristic geometry of the axon hillock by tapering the first 10 μm of the axon from 4 to 1 μm, and (iii) setting the density of sodium channels in the hillock to intermediate between the soma and the axon, a half of the density in the AIS (for sodium channels in the soma, the hillock and the AIS, the density ratio was 1:5:10, or 800, 4000 and 8000 pS/μm^2). The APs simulated with this model had smooth onset dynamics, perfectly fitted by an exponent as indicated by a low (0.22) ratio of fit errors (Fig. 8E, brown diamond; see also Supplementary Fig. S5). These results confirm the notion that the geometrical arrangement of the axon and

the soma do influence the AP onset dynamics in the invasion-based models.

Onset dynamics of somatic APs in morphologically realistic neuron models

To quantify the onset dynamics of APs in neuron models with realistic morphology, we used models of layer 5 pyramidal neuron, layer 3 pyramidal neuron, layer 3 aspiny cell and layer 4 spiny stellate cell (Mainen et al., 1995; Mainen and Sejnowski, 1996) available at SenseLab's ModelDB database, URL: http://senselab.med.yale.edu/senselab/modeldb. All these models employ HH sodium channels. In these models, the original distributions of conductances in the cell was either left unchanged (Mainen et al., 1995; Mainen and Sejnowski, 1996), or modified according to the published models (see below). Fig. 8A1–C1 shows an AP simulated with a layer 5 pyramidal cell model with the original distribution of sodium conductances: low in the soma and dendrites (20 pS/μm^2, or 2 mS/cm^2), and 1500 times higher (30,000 pS/μm^2, or 3000 mS/cm^2) in the AIS (Mainen et al., 1995; Mainen and Sejnowski, 1996). In this model, the AP is initiated in the axon and backpropagates antidromically into the soma. Despite the extremely high density of sodium channels in the axon, the onset of the somatic AP is relatively smooth, better fitted by an exponential than by a piecewise linear function (the ratio of fit errors 0.82). We also evaluated the AP initiation dynamics in the model of layer 5 pyramidal cell with the same morphology but altered distribution of sodium and potassium channels. Fig. 8A2–C2 shows an AP simulated in the model with sodium and potassium conductances suggested in a study reproducing the firing patterns of neocortical neurons (Destexhe and Pare, 1999; Destexhe et al., 2001). The AP produced by this model has a smooth onset with the ratio of fit errors 0.13 (Fig. 8C2). Fig. 8A3–C3 shows the results of simulations in which sodium channels in the AIS reproduced the experimentally reported values: their density was three times higher and the activation curve was shifted by 8 mV to the left (towards hyperpolarizing values) compared to the somatic channels (Colbert and Pan, 2002; Kole et al., 2008). This AP has a smooth onset too, and the ratio of fit errors is 0.01 (Fig. 8C3). The similarly smooth AP onset dynamics was observed also in morphologically realistic models of layer 3 pyramidal neuron. Both the original model (Mainen et al., 1995; Mainen and Sejnowski, 1996) as well as the model with sodium and potassium conductances modified to reproduce the firing patterns of neocortical neurons (Destexhe and Pare, 1999; Destexhe et al., 2001), generated APs with smooth onset dynamics (Fig. 8A4–C4, A5–C5). Zoom in of the initial portions of the phase plots of these five APs confirm their slow onset dynamics (Fig. 8D).

The results of quantification of the onset dynamics of APs simulated with the morphologically realistic models, including the models of layer 3 and 5 pyramids described in the previous paragraph, and the simple model used in (Yu et al., 2008) are summarized in Fig. 8E. All these models produced APs with smooth onset dynamics that were well fitted with an exponential function and thus the ratio of fit errors was <1, well below the values measured in the recorded neocortical neurons (Fig. 8E). The AP onset was somewhat sharper in the simple model used in (Yu et al., 2008), due to its artificial geometry discussed above. But even this model generated APs with a smooth onset, as soon as it's axon geometry was made more realistic.

Dependence of the AP onset dynamics on temperature

All simulations described so far were performed at virtual temperature 32 °C. We opted for using 32 °C, and not higher temperature in the simulations for the following reasons. First, most of experimental data used as a reference (Volgushev et al., 2008) were recorded at 30–32 °C. Second, kinetics of sodium channel activation is usually studied at even lower temperatures, below 25 °C (Neumcke and Stampfli, 1982; Huguenard et al., 1989; Kuo and Bean, 1994; Martina and Jonas, 1997; Hille, 2001; Baranauskas and Martina, 2006; Baranauskas, 2007). Finally, the step-like kink at the onset of neocortical APs is clearly present both at room temperature and at physiological temperature range (Naundorf et al., 2006; Volgushev et al., 2008).

Previous studies demonstrated that temperature has profound effects on the AP amplitude and width, as well as on the excitability, repetitive firing and passive properties of neocortical neurons (Klee et al., 1974; Thompson et al., 1985; Volgushev et al., 2000a,b; Trevelyan and Jack, 2002). A strong temperature dependence of channel kinetics is implemented in the models, for example (Mainen et al., 1995; Mainen and Sejnowski, 1996; Yu et al., 2008). To test how the AP onset dynamics in the models is affected by the virtual temperature, we made an additional series of simulations. We used the combinations of parameters that at 32 °C produced somatic APs with a sharp onset dynamics, quantitatively compatible with the experimental data. For these models, we performed simulations at different virtual temperatures, from 10 to 37 °C. Temperature dependence of passive cell properties, the membrane capacitance C_m ($Q_{10}=0.96$), the axial resistance Rax ($Q_{10}=0.8$) and the leak conductance G_{Leak} ($Q_{10}=1.97$) was implemented in the models according to (Trevelyan and Jack, 2002). Fig. 9 shows the temperature dependence of the AP onset dynamics in four models that produced sharp AP onsets at 32 °C, and in neocortical neurons recorded in slices. In all four models, a combination of a high cytoplasmic resistance (Rax=400 Ohm×cm), narrow axon initial segment (AIS diameter 1 μm) and high sodium channel density in the AIS (50, 100 and 300 times higher than in the soma for HH models, gNa=5000, 10,000 and 30,000 pS/μm^2 and 100 times higher than in the soma for BM model, gNa=10,000 pS/μm^2) were used.

An increase of the temperature from 32 to 37 °C led to a yet sharper onset dynamics in all four models. Notably, the HH model with Rax=400 Ohm×cm, 1 μm AIS diameter and gNa=5000 pS/μm^2, which at 32 °C generated APs with onset dynamics just within the experimentally observed range (error ratio 3.59), at 37 °C generated APs

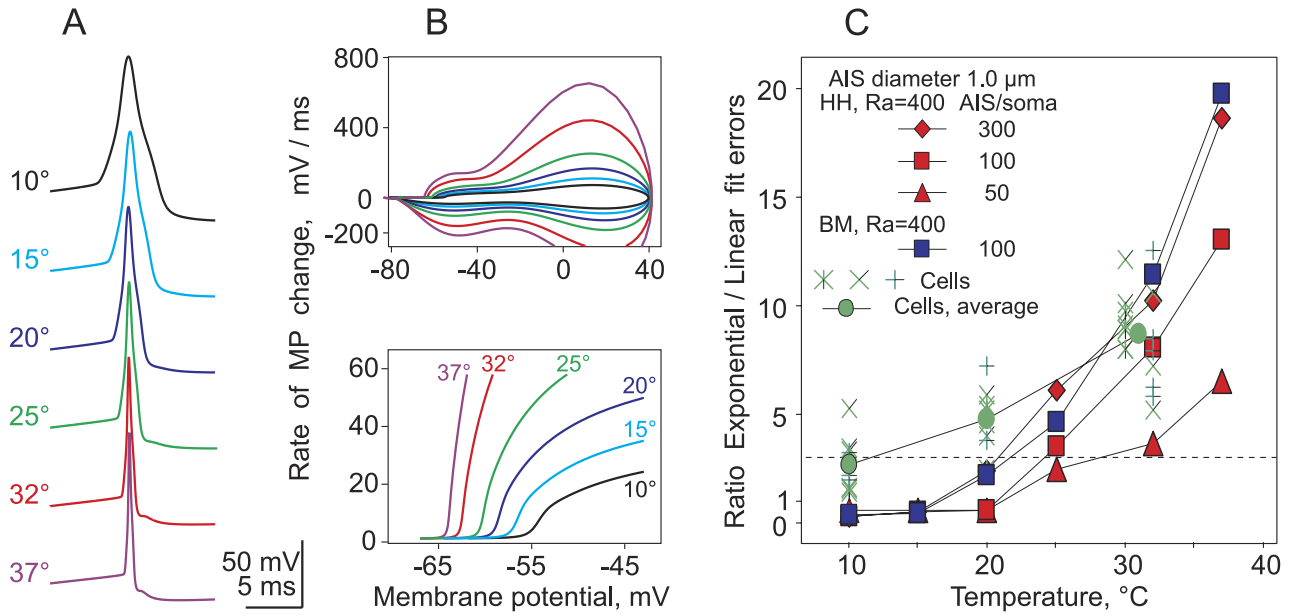

Fig. 9. Temperature dependence of the AP onset dynamics in models and recorded neurons. (A) APs simulated with a model with HH sodium channels, AIS/soma ratio of sodium channels 100 and cytoplasmic resistance 400 Ohm×cm at different temperatures. (B) Phase plots and zoom in of the initial portions of phase plots of APs from (A). (C) Dependence of the ratio of errors of exponential to linear fits on temperature for four models and three neurons recorded in rat neocortical slices. Red symbols: models with HH sodium channels, AIS diameter 1 μm, cytoplasmic resistance 400 Ohm×cm and ratio of AIS/soma sodium channels 50, 100 and 300. Blue squares: model with BM sodium channels, AIS diameter 1 μm, cytoplasmic resistance 400 Ohm×cm and ratio of AIS/soma sodium channels 100. Green symbols: rat neocortex neurons, line symbols represent individual cells and measurements, green circles connected with the line show average data for these cells. Note that vertical axis in this plot reaches higher values than in other figures. For interpretation of the references to color in this figure legend, the reader is referred to the Web version of this article.

with onset dynamics well within the experimental distribution (error ratio 6.46, Fig. 9A, B and red triangles in C). However, in all four models lowering the temperature to 20 °C made the AP onset dynamics considerably slower and in the models with density of HH channels in the AIS 50 or 100 times higher than in the soma, the generated APs had a smooth onset (Fig. 9C). A further lowering of temperature to 15 °C and 10 °C, resulted in a smooth AP onset in all four models (Fig. 9C). The pronounced dependence of the onset dynamics of simulated APs on temperature may be one further reason for discrepancy between the conclusions reached in the paper reporting simulations at 37 °C (Yu et al., 2008) and results of the present study.

The recording temperature affected also the onset dynamics of APs in rat neocortical neurons, but the temperature dependence of the AP onset dynamics was not as dramatic in neurons as in the simulations. Lowering the recording temperature from 30–32°C to 20 °C and 10 °C led to a slower onset. However, the onset still expressed a clear step-like kink at 20 °C in all recorded cells, and in some cells even at 10 °C (Fig. 9C, green symbols).

DISCUSSION

Here we demonstrate with two Hodgkin and Huxley type sodium channel models, the canonical (Hodgkin and Huxley, 1952a,b; Hodgkin et al., 1952) and the modified version with much faster onset kinetics (Baranauskas and Martina, 2006), that the initiation of an AP in the axon initial segment and its backpropagation to the soma do not necessarily lead to the sharp AP onset in the soma. For a broad range of parameters, such models could reproduce the distal AP initiation and backpropagation, but failed to quantitatively reproduce the onset dynamics of somatic APs observed in cortical neurons. This failure to reproduce the sharp AP onset dynamics in the models cannot be attributed to our choice of the two sodium channel models. The HH and BM models represent two extremes suggested to reproduce sodium current kinetics in central neurons (Kole et al., 2008; Engel and Jonas, 2005) and models with BM channels generate APs with faster onsets than any other tested model. Thus, we conclude that, in order to explain the rapid AP onset in the soma in the invasion scenario, the backpropagation of an AP from the AIS into the soma represents a necessary but not sufficient condition. Below we will discuss the ranges of parameters that can produce the somatic AP onset as sharp as seen in neurons.

Factors determining the AP onset dynamics in the soma

In layer 5 pyramidal cells in the neocortex, APs are initiated in the axon initial segment, propagate orthodromically down the axon and backpropagate antidromically into the soma and dendrites (Stuart and Sakmann, 1994; Stuart et al., 1997a,b). The initiation site is located about 25–35 μm from the axon hillock in layer 5 pyramids from rat somatosensory cortex (Palmer and Stuart, 2006; Kole et al., 2008), or about 40 μm from the soma in layer 5 pyramids

from prefrontal or somatosensory ferret cortex (Yu et al., 2008). Since an AP is not initiated in the soma, the onset of the somatic AP is determined not by local active currents but by the so-called Iprop current (Yu et al., 2008) that travels to the soma from the AP initiation site. The depolarization caused by Iprop starts before any appreciable activation of local voltage-gated channels. Except for channels that are already open, activation of any channels is not fast enough to alter the travel and the shape of Iprop. Once an AP is initiated, the Iprop effects are, in essence, a passive phenomenon. This explains why neither the persistent sodium current nor the voltage activated potassium currents had any noticeable effect on the AP onset dynamics. In contrast, the AIS diameter and the axonal cytoplasmic resistance, two passive parameters, had a very strong impact on the AP onset dynamics. Yet, sodium channels generating an AP in the AIS do determine the initial Iprop amplitude and dynamics, making the density of Na channels in the AIS, the kinetics of these channels and its temperature dependence important determinants of the AP onset dynamics in the soma.

Notably, just the presence of the invasion current Iprop is not sufficient to produce a step-like kink at the onset of somatic AP. In a broad range of models analyzed here, as well as in the models suggested earlier to explain axonal AP initiation, for example (Colbert and Pan, 2002; Schmidt-Hieber et al., 2008a), the onset of AP in the soma is smooth, despite an invasion of an AP initiated in the AIS. In the models with a wide AIS ($>$1.5 μm) or low cytoplasmic resistance ($<$200 Ohm$\times$cm), which might enhance Iprop component, the onset of somatic AP remained perfectly smooth despite the presence of high density sodium channels in the AIS (gNa up to 90,000 pS/μm^2). To make the onset of somatic AP sharp, the dynamics of Iprop produced by strong sodium currents at the initiation site should be modified on the way to the soma. Such a modification of Iprop dynamics in the models with gNa in the AIS $>\sim$10,000 pS/μm^2 could be achieved by a high cytoplasmic resistance$>\sim$300 Ohm$\times$cm, or small diameter $<\sim$1 μm of the AIS. Combination of both small axon diameter ($\leq$1 μm) and high cytoplasmic resistance ($\geq$400 Ohm$\times$cm) reduces the requirement to gNa in the AIS to $\sim$5000 pS/μm^2 (Fig. 10).

Thus, we identified the following parameters, which are critical for determining the onset dynamics of the simulated somatic APs: (i) the high absolute sodium channel density in the AIS, which is necessary to generate strong current at the initiation site and produce strong Iprop, (ii) the high axonal cytoplasmic resistance and/or the small AIS diameter, which are necessary to modify the onset of Iprop on its way to the soma, and (iii) the temperature which influences the amplitude and kinetics of sodium currents due to steep temperature dependences implemented in sodium channel models.

Below we will compare the parameter ranges that were necessary to reproduce the AP onset as rapid as observed in neurons and the restrictions imposed by experimental data on the ranges of these parameters. The ratio of fit errors of 3 will be used as a threshold value because, in our sample of 49 neocortical neurons (data from Volgushev et al., 2008), APs from all but one neuron had the ratio of fit errors $>$3 (see Fig. 3E). Since the measure of AP onset dynamics (the ratio of fit errors) changed monotonically with all these parameters, we can determine the "threshold" values that must be met or exceeded in order to reproduce the rapid AP onset in simulations. It is important to note that a threshold value for each single parameter is affected by the settings of the remaining parameters. Therefore, we will delineate a region in multi-dimensional parameter space, in which the ratio of fit errors is $>$3 (Fig. 10). Since our experimental data on the AP onset dynamics was largely obtained at 32 °C, we will start the comparison for simulations results attained at 32 °C while the temperature effects will be discussed afterwards.

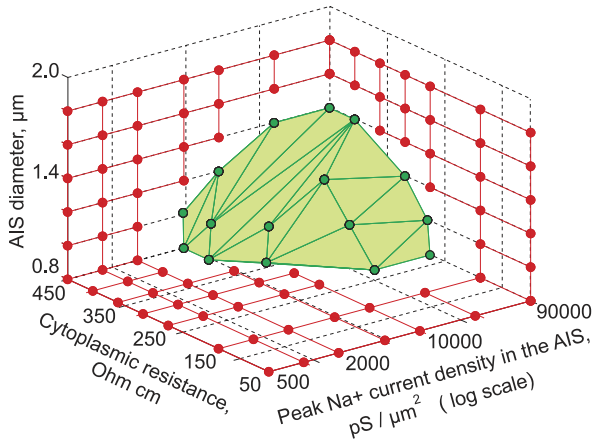

Fig. 10. Parameter combinations required to reproduce the sharp onset of somatic AP in the invasion scenario. 3D plot shows the space of parameters (peak Na^+ current density in the AIS, cytoplasmic resistance and AIS diameter) tested. Circles show projections of the tested parameter values on the surfaces; all their combinations within the plot volume were tested too, but are not plotted for clarity. Green circles and green surface delimit the portion of parameter space in which APs in the soma had sharp onset (ratio of fit errors $>$3). In the remaining portion of parameter space, the onset of somatic APs was smooth (ratio of fit errors $<$3), projections of these parameter combinations on the surfaces are shown as red circles. For interpretation of the references to color in this figure legend, the reader is referred to the Web version of this article.

Requirements of the invasion hypothesis to morphological and electrophysiological properties of the AIS

The AIS morphology was well-described in a number of careful electron microscopy and imaging studies. In neocortical pyramidal neurons, the AIS originates from the axon hillock and is about 40–50 μm long (Sloper and Powell, 1979; Palmer and Stuart, 2006) and 1–3.3 μm in diameter (Sloper and Powell, 1979). In other cell types, the AIS is similar in length, approximately 30–55 μm (Sloper and Powell, 1979), but narrower, approximately 0.6 to 1.7 μm, the AIS diameter correlating with the soma size (Peters et al., 1968). In our simulations, we changed the AIS diameters from 0.8 to 1.8 μm. A further increase in the diameter was not tested because in models with AIS di-

ameter ≥1.6 μm the AP onset remained smooth even for the highest tested values of axial resistance (450 Ohm×cm) and sodium current densities in the AIS (90,000 pS/μm^2). No experimental data indicates such high values of axial resistance or supports the presence of such high densities of sodium channels in the AIS (see below).

No direct data is available on axial resistance in the axons of cortical neurons and we can only rely on the estimates based on the cable properties of the dendrites in central neurons (150–200 Ohm×cm, Stuart and Spruston, 1995, 1998; Meyer et al., 1997; Trevelyan and Jack, 2002) or the measurements made in the squid giant axon (~60 Ohm×cm, Roth and Wikswo (1985)). The ion concentration in the squid axon is higher than in the cytoplasm of central neurons, resulting in higher cytoplasmic resistance in the central neurons. For this reason, the values from central neuron dendrites are usually used in simulations (e.g. Mainen et al., 1995; Mainen and Sejnowski, 1996; Destexhe and Pare, 1999; Migliore et al., 1999; Destexhe et al., 2001; Colbert and Pan, 2002; Shu et al., 2006; McCormick et al., 2007; Yu et al., 2008). In summary, we think it is safe to state that the axonal internal resistance does not exceed 450 Ohm×cm and the most likely value is somewhere between 150 and 300 Ohm×cm.

The most contentious issue is the sodium channel density in the AIS. Measurements of sodium currents in membrane patches taken from the AIS revealed sodium channel densities two to five times higher than in the soma (Colbert and Johnston, 1996; Colbert and Pan, 2002; Schmidt-Hieber et al., 2008b), even after the destruction of actin filaments that may normally prevent the channel entrance into the recorded patch (Kole et al., 2008). Estimates of the peak density of sodium current in the AIS, based on the above direct data, resulted in moderate values of <1000 pS/μm^2 (Colbert and Johnston, 1996; Colbert and Pan, 2002; Schmidt-Hieber et al., 2008b). Estimates based on recordings from injury induced blebs of cut axons gave higher estimates, up to ~3200 pS/μm^2 (Hu et al., 2009). Estimates from the sodium imaging data and their computational analysis indicated a density of ~2500 pS/μm^2 (Kole et al., 2008). Phenomenological adjustment of computational models to reproduce the experimentally observed site of AP initiation and the maximal rate of rise of somatic AP suggested a broader range of sodium channel densities in the AIS, from ~1000 pS/μm^2 (Colbert and Pan, 2002; Schmidt-Hieber et al., 2008b) to 8000 pS/μm^2 (Yu et al., 2008). All these estimates are compatible with immunohistochemical data, which reveal higher density of sodium channels in the AIS than in the soma (Komada and Soriano, 2002; Inda et al., 2006; Kole et al., 2008; Lorincz and Nusser, 2008; Hu et al., 2009). Since the highest recent estimate of the peak sodium current density in the AIS is 8000 pS/μm^2, we consider it is safe to state that the peak density of sodium current in the AIS is below 10,000 pS/μm^2.

The summary of parameter space used in the simulations and the portion of this space in which a sharp somatic APs can be produced in the invasion scenario is shown in Fig. 10. In brief, we found that for cells with the AIS diameter of ≥1.6 μm even a combination of the high axonal cytoplasmic resistance (450 Ohm×cm) and the highest sodium channel density (90,000 pS/μm^2) tested was insufficient to attain the rapid AP onset. For the AIS of 1.4 μm in diameter, the sodium channel density of 30,000 pS/μm^2 combined with axial resistance ≥400 Ohm×cm were necessary to attain the sharp somatic AP onset dynamics with the ratio of fit errors >3. The narrow AIS of 0.8 or 1.0 μm required sodium channel densities of >5000 pS/μm^2 in the AIS for the axial resistance of 400 Ohm×cm but for a lower axial resistance of 250 Ohm×cm this minimal gNa in the AIS was 30,000 pS/μm^2. Notably, for models with axial resistance <250 Ohm×cm, or gNa in the AIS <5000 pS/μm^2, the onset of APs remained smooth with any combination of other parameters.

These specific requirements to model parameters that are necessary for reproducing the sharp somatic AP onset dynamics in the invasion scenario are clearly different from the experimentally determined values and disagree with the recent claim that the rapid onset of somatic APs is typical for models initiating APs not in the soma but at some distance from it down the axon initial segment (Yu et al., 2008). Several possible reasons may underlie this latter discrepancy. First, we used different measures of AP onset dynamics. As we have shown in the results, raising the threshold for calculation of the AP "rapidness" artificially diminishes the difference in this measure between a smooth, exponential-like and a steep, step-like onset dynamics. Second, in contrast to our "range testing" approach, Yu and colleagues tested very few different models of neurons with carefully selected parameters. For example, in their simple cell model, a narrow, 1 μm in diameter axon is attached directly to the soma without a hillock. Our simulations show that the restoration of axonal morphology consistent with morphological data results in a smooth onset of somatic APs in this model. Thus, both the results presented here and in (Yu et al., 2008) show that when APs are initiated 30–40 μm down the AIS, invasion scenario can produce a kink at the onset of somatic AP only in models with carefully selected parameters. In the present paper, we have identified the limits for parameters and their combinations within which the invasion scenario is able to explain the rapid onset of somatic APs.

Can the simulations and the experimental data be reconciled?

The above brief overview of experimental and simulation data reveals discrepancies between the parameter ranges within which the rapid AP onset is reproduced in the invasion scenario and the ranges of the same parameters deduced from the available experimental data on the AIS properties in neocortical neurons. These requirements to the specific parameter combinations that may at best be met in some marginal cases, are in a marked contrast to the fact that somatic APs in different types of neocortical neurons always exhibit step-like onset dynamics (Naundorf et al., 2006; Yu et al., 2008). Therefore, we should be able to find an explanation for the discrepancies between simulation and experimental parameter values. If not, ad-

ditional mechanisms other than just the invasion scenario are needed to account for the sharp onset of APs in neocortical neurons.

To reconcile the experimental and simulation data, one possibility could be that the effective AIS diameter is in fact smaller than reported by the electron microscopy studies. Changes in the AIS diameter have a strong impact on the somatic AP onset dynamics. Although the electron microscopy data provide very precise dimensions of the AIS (Peters et al., 1968; Sloper and Powell, 1979), it is possible that a diffusion barrier in the AIS (Winckler et al., 1999) increases the resistance along the AIS and decreases the effectively conducting AIS diameter. While a dense cytoskeleton with anchored to membrane proteins can hinder diffusion of large membrane-associated molecules along the AIS membrane (Winckler et al., 1999), it is unlikely to significantly reduce the effective axon diameter and obstruct the movement of small ions to the extent that would significantly speed up the AP onset.

One further possibility is indicated by a recent study that claims to identify analytically the range of synaptic noise strength with which a single-compartment Hodgkin and Huxley model can reproduce the steep AP onset seen in neurons (Colwell and Brenner, 2009). However, our control experimental data set was obtained in slices *in vitro* where the background synaptic activity is minimal and for sure does not reach the values suggested by the Colwell and Brenner (2009) model. Hence, synaptic noise cannot explain the abovementioned discrepancies between experimental observations and existing neuron models.

The most difficult task is to reconcile the simulation and experimental data on the temperature effects on AP onset dynamics. Although in the simulations, the temperature effects on the AP onset dynamics are indirect, that is via the kinetics of sodium channels, changes in virtual temperature have a dramatic impact on the ratio of fit errors. In simulations, even for extreme sets of parameters the somatic AP onset dynamics was always slow at room temperature. In contrast, in neurons APs exhibit a rapid onset dynamics at room temperature (Naundorf et al., 2006; Volgushev et al., 2008), and in some cells the somatic AP onset remains step-like even at 10 °C (Fig. 9). In the recorded neurons, the AP onset dynamics changed little with temperature above 20 °C suggesting that the process is saturated. The available experimental data on the kinetics of sodium channel activation is most reliable for temperatures below 25 °C (Neumcke and Stampfli, 1982; Huguenard et al., 1989; Kuo and Bean, 1994; Martina and Jonas, 1997; Hille, 2001; Baranauskas and Martina, 2006; Baranauskas, 2007) suggesting that simulation results at low temperatures may be more reliable than at 37 °C. We note however, that the largest differences between the experimental and simulation data are found for low temperatures and we have no explanation for this observation.

CONCLUSION

To conclude, we have identified significant differences between the sets of AIS parameters required to reproduce the rapid AP onset in the invasion scenario and the currently accepted and experimentally estimated values of these parameters. The specificity of requirements for parameter combinations, which are necessary for reproducing the sharp onset of somatic AP in the invasion scenario, is in a marked contrast to the common occurrence of the step-like onset dynamics of APs in different types of neocortical neurons. To the best of our knowledge, there is no simple explanation to account for clearly different temperature dependence of the AP onset dynamics in the models and real neurons. Further experiments are needed to explain the sharp onset dynamics of cortical APs and the discrepancies between the simulations and experimental data.

Acknowledgments—We are grateful to Marina Chistiakova, Alexey Malyshev, Heather Read and James Chrobak for discussions and comments and Heather Read and James Chrobak for improving the English. Supported by the BMBF, grant 01GQ07112 (MV, FW), GIF grant 906-17.1/2006 (MV, FW) and University of Connecticut, startup funds and grant IFP-090051 to MV.

REFERENCES

Astman N, Gutnick MJ, Fleidervish IA (2006) Persistent sodium current in layer 5 neocortical neurons is primarily generated in the proximal axon. J Neurosci 26:3465–3473.

Baranauskas G, Martina M (2006) Sodium currents activate without a Hodgkin-and-Huxley-type delay in central mammalian neurons. J Neurosci 26:671–684.

Baranauskas G (2007) Ionic channel function in action potential generation: current perspective. Mol Neurobiol 35:129–150.

Bekkers JM, Stevens CF (1996) Cable properties of cultured hippocampal neurons determined from sucrose-evoked miniature EPSCs. J Neurophysiol 75:1250–1255.

Bragina TA (1986) Synapse ultrastructure of the initial axon segment of the pyramidal neuron. Neurosci Behav Physiol 16:1–6.

Buracas GT, Albright TD (1999) Gauging sensory representations in the brain. Trends Neurosci 22:303–309.

Carnevale NT, Hines ML (2006) The NEURON Book, pp 457. Cambridge, UK: Cambridge University Press.

Clark BA, Monsivais P, Branco T, London M, Häusser M (2005) The site of action potential initiation in cerebellar Purkinje neurons. Nat Neurosci 8:137–139.

Colbert CM, Johnston D (1996) Axonal action-potential initiation and Na+ channel densities in the soma and axon initial segment of subicular pyramidal neurons. J Neurosci 16:6676–6686.

Colbert CM, Pan E (2002) Ion channel properties underlying axonal action potential initiation in pyramidal neurons. Nat Neurosci 5:533–538.

Colwell LJ, Brenner MP (2009) Action potential initiation in the Hodgkin–Huxley model. PLoS Comput Biol 5:e1000265.

Dayan P, Abbott LF (2001) Theoretical neuroscience, pp 460. Cambridge, MA: MIT Press.

Dekker JP, Yellen G (2006) Cooperative gating between single HCN pacemaker channels. J Gen Physiol 128:561–567.

Destexhe A, Pare D (1999) Impact of network activity on the integrative properties of neocortical pyramidal neurons *in vivo*. J Neurophysiol 81:1531–1547.

Destexhe A, Rudolph M, Fellous JM, Sejnowski TJ (2001) Fluctuating synaptic conductances recreate in vivo-like activity in neocortical neurons. Neuroscience 107:13–24.

Engel D, Jonas P (2005) Presynaptic action potential amplification by voltage-gated Na channels in hippocampal mossy fiber boutons. Neuron 45:405–417.

Fourcaud-Trocme N, Hansel D, van Vreeswijk C, Brunel N (2003) How spike generation mechanisms determine the neuronal response to fluctuating inputs. J Neurosci 23:11628–11640.

Hille B (2001) Ion channels of excitable membranes, pp 813. Sunderland, MA: Sinauer Associates, Inc.

Hines ML, Morse T, Migliore M, Carnevale NT, Shepherd GM (2004) Model DB: a database to support computational neuroscience. J Comput Neurosci 17:7–11.

Hodgkin AL, Huxley AF (1952a) A quantutative description of membrane current and its application to conduction and axcitation in nerve. J Physiol 117:500–544.

Hodgkin AL, Huxley AF (1952b) Currents carried by sodium and potassium ions through the membrane of the giant axon of *loligo*. J Physiol 116:449–472.

Hodgkin AL, Huxley AF, Katz B (1952) Measurement of current-voltage relations in the membrane of the giant axon of *Loligo*. J Physiol 116:424–448.

Hu W, Tian C, Li T, Yang M, Hou H, Shu Y (2009) Distinct contributions of Nav1.6 and Nav1.2 in action potential initiation and backpropagation. Nat Neurosci 12:996–1002.

Huguenard JR, Hamill OP, Prince DA (1989) Sodium channels in dendrites of rat cortical pyramidal neurons. Proc Natl Acad Sci U S A 86:2473–2477.

Inda MC, DeFelipe J, Munoz A (2006) Voltage-gated ion channels in the axon initial segment of human cortical pyramidal cells and their relationship with chandelier cells. Proc Natl Acad Sci U S A 103:2920–2925.

Kampa BM, Letzkus JJ, Stuart GJ (2007) Dendritic mechanisms controlling spike-timing-dependent synaptic plasticity. Trends Neurosci 30:456–463.

Khaliq ZM, Raman IM (2006) Relative contributions of axonal and somatic Na channels to action potential initiation in cerebellar Purkinje neurons. J Neurosci 26:1935–1944.

Klee MR, Pierau FK, Faber DS (1974) Temperature effects on resting potential and spike parameters of cat motoneurons. Exp Brain Res 19:478–492.

Kole MH, Ilschner SU, Kampa BM, Williams SR, Ruben PC, Stuart GJ (2008) Action potential generation requires a high sodium channel density in the axon initial segment. Nat Neurosci 11:178–186.

Kole MH, Letzkus JJ, Stuart GJ (2007) Axon initial segment Kv1 channels control axonal action potential waveform and synaptic efficacy. Neuron 55:633–647.

Kole MH, Stuart GJ (2008) Is action potential threshold lowest in the axon? Nat Neurosci 11:1253–1255.

Komada M, Soriano P (2002) βIV-spectrin regulates sodium channel clustering through ankyrin-G at axon initial segments and nodes of Ranvier. J Cell Biol 156:337–348.

Korngreen A, Sakmann B (2000) Voltage-gated K+ channels in layer 5 neocortical pyramidal neurones from young rats: subtapes and gradients. J Physiol 525:621–639.

Kress GJ, Dowling MJ, Meeks JP, Mennerick S (2008) High threshold, proximal initiation, and slow conduction velocity of action potentials in dentate granule neuron mossy fibers. J Neurophysiol 100:281–291.

Kuo CC, Bean BP (1994) Na+ channels must deactivate to recover from inactivation. Neuron 12:819–829.

Lorincz A, Nusser Z (2008) Cell-type-dependent molecular composition of the axon initial segment. J Neurosci 28:14329–14340.

Magee JC, Johnston D (1997) A synaptically controlled, associative signal for Hebbian plasticity in hippocampal neurons. Science 275:209–213.

Mainen ZF, Joerges J, Huguenard JR, Sejnowski TJ (1995) A model of spike initiation in neocortical pyramidal neurons. Neuron 15:1427–1439.

Mainen ZF, Sejnowski TJ (1996) Influence of dendritic structure on firing pattern in model neocortical neurons. Nature 382:363–366.

Markram H, Luebke J, Frotscher M, Sakmann B (1997) Regulation of synaptic efficacy by coincidence of postsynaptic APs and EPSPs. Science 275:213–215.

Martina M, Jonas P (1997) Functional differences in Na+ channel gating between fast-spiking interneurons and principal neurones of rat hippocampus. J Physiol 505:593–603.

Marx SO, Gaburjakova J, Gaburjakova M, Henrikson C, Ondrias K, Marks AR (2001) Coupled gating between cardiac calcium release channels ryanodine receptors. Circ Res 88:1151–1158.

Marx SO, Ondrias K, Marks AR (1998) Coupled gating between individual skeletal muscle Ca2+ release channels ryanodine receptors. Science 281:818–821.

McCormick DA, Shu Y, Yu Y (2007) Hodgkin and Huxley model—still standing? Arising from: Naundorf et al., Nature 440:1060–1063. Nature 445:E1–E2.

Meeks JP, Jiang X, Mennerick S (2005) Action potential fidelity during normal and epileptiform activity in paired soma-axon recordings from rat hippocampus. J Physiol 566:425–441.

Meyer E, Muller CO, Fromherz P (1997) Cable properties of dendrites in hippocampal neurons of the rat mapped by a voltage-sensitive dye. Eur J Neurosci 9:778–785.

Migliore M, Hoffman DA, Magee JC, Johnston D (1999) Role of an A-type K+ conductance in the back-propagation of action potentials in the dendrites of hippocampal pyramidal neurons. J Comput Neurosci 7:5–15.

Miller M, Peters A (1981) Maturation of rat visual cortex: part II. A combined Golgi-electron microscope study of pyramidal neurons. J Comp Neurol 203:555–573.

Molina ML, Barrera FN, Fernandez AM, Poveda JA, Renart ML, Encinar JA, Riquelme G, Gonzalez-Ros JM (2006) Clustering and coupled gating modulate the activity in KcsA, a potassium channel model. J Biol Chem 281:18837–18848.

Naundorf B, Geisel T, Wolf F (2005) Action potential onset dynamics and the response speed of neuronal populations. J Comput Neurosci 18:297–309.

Naundorf B, Wolf F, Volgushev M (2006) Unique features of action potential initiation in cortical neurons. Nature 440:1060–1063.

Neumcke B, Stampfli R (1982) Sodium currents and sodium-current fluctuations in rat myelinated nerve fibres. J Physiol 329:163–184.

Palmer LM, Stuart GJ (2006) Site of action potential initiation in layer 5 pyramidal neurons. J Neurosci 26:1854–1863.

Patlak J (1991) Molecular kinetics of voltage-dependent Na+ channels. Physiol Rev 71:1047–1080.

Peters A, Proskauer CC, Kaiserman-Abramof IR (1968) The small pyramidal neuron of the rat cerebral cortex: the axon hillock and initial segment. J Cell Biol 39:604–619.

Roth BJ, Wikswo JP Jr (1985) The magnetic field of a single axon: a comparison of theory and experiment. Biophys J 48:93–109.

Schmidt-Hieber C, Jonas P, Bischofsberger J (2008a) Action potential initiation and propagation in hippocampal mossy fibre axons. J Physiol 586:1849–1857.

Schmidt-Hieber C, Jonas P, Bischofsberger J (2008b) Differential sodium channel gating in soma and axon of hippocampal granule cells. Soc Neurosci Abstr 535:2.

Shu Y, Duque A, Yu Y, Haider B, McCormick DA (2007) Properties of action potential initiation in neocortical pyramidal cells: evidence from whole cell axon recordings. J Neurophysiol 97:746–760.

Shu Y, Hasenstaub A, Duque A, Yu Y, McCormick DA (2006) Modulation of intracortical synaptic potentials by presynaptic somatic membrane potential. Nature 441:761–765.

Singer W (1999) Neuronal synchrony: a versatile code for the definition of relations? Neuron 24:49–65.

Sloper JJ, Powell TP (1979) A study of the axon initial segment and proximal axon of neurons in the primate motor and somatic sensory cortices. Philos Trans R Soc Lond B Biol Sci 285:173–197.

Stuart G, Spruston N (1995) Probing dendritic function with patch pipettes. Curr Opin Neurobiol 5:389–394.

Stuart G, Spruston N (1998) Determinants of voltage attenuation in neocortical pyramidal neuron dendrites. J Neurosci 18:3501–3510.
Stuart G, Häusser M (1994) Initiation and spread of sodium action potentials in cerebellar Purkinje cells. Neuron 13:703–712.
Stuart G, Sakmann B (1994) Active propagation of somatic action potentials into neocortical pyramidal cell dendrites. Nature 367:69–72.
Stuart G, Schiller J, Sakmann B (1997a) Action potential initiation and propagation in rat neocortical pyramidal neurons. J Physiol Lond 505:617–632.
Stuart G, Spruston N, Sakmann B, Häusser M (1997b) Action npotential initiation and backpropagation in neurons of the mammalian CNS. Trends Neurosci 20:125–131.
Thompson SM, Masukawa LM, Prince DA (1985) Temperature dependence of intrinsic membrane properties and synaptic potentials in hippocampal CA 1 neurons in vitro. J Neurosci 5:817–824.
Trevelyan AJ, Jack JJ (2002) Detailed passivce cable models of layer 2/3 pyramidal cells in rat visual cortex at different temperatures. J Physiol 539:623–636.
Undrovinas AI, Fleidervish IA, Makielski JC (1992) Inward sodium current at resting potentials in single cardiac myocytes induced by the ischemic metabolite lysophosphatidylcholine. Circ Res 71:1231–1241.
Volgushev M, Malyshev A, Balaban P, Chistiakova M, Volgushev S, Wolf F (2008) Onset dynamics of action potentials in rat neocortical neurons and identified snail neurons: quantification of the difference. PLoS ONE 3:e1962.
Volgushev M, Vidyasagar TR, Chistiakova M, Eysel UT (2000a) Synaptic transmission in the neocortex during reversible cooling. Neuroscience 98:9–22.
Volgushev M, Vidyasagar TR, Chistiakova M, Yousef T, Eysel UT (2000b) Membrane properties and spike generation in rat visual cortical cells during reversible cooling. J Physiol 522(1):59–76.
Winckler B, Forscher P, Mellmann I (1999) A diffusion barrier maintains distribution of membrane proteins in polarized neurons. Nature 397:698–701.
Yu Y, Shu Y, McCormick DA (2008) Cortical action potential backpropagation explains spike threshold variability and rapid-onset kinetics. J Neurosci 28:7260–7272.
Yuan LL, Chen X (2006) Diversity of potassium channels in neuronal dendrites. Prog Neurobiol 78:374–389.

APPENDIX

Supplementary data

Supplementary data associated with this article can be found, in the online version, at doi:10.1016/j.neuroscience.2010.02.072.

(Accepted 25 February 2010)
(Available online 6 March 2010)